Taylor & Francis
Taylor & Francis Group

Journal of Earthquake Engineering

ISSN: 1363-2469 (Print) 1559-808X (Online) Journal homepage: http://www.tandfonline.com/loi/ueqe20

Direct Displacement-Based Seismic Design of Eccentrically Braced Steel Frames

Gerard J. O'Reilly & Timothy J. Sullivan

To cite this article: Gerard J. O'Reilly & Timothy J. Sullivan (2016) Direct Displacement-Based Seismic Design of Eccentrically Braced Steel Frames, Journal of Earthquake Engineering, 20:2, 243-278, DOI: 10.1080/13632469.2015.1061465

To link to this article: https://doi.org/10.1080/13632469.2015.1061465

Accepted author version posted online: 04 Sep 2015.
Published online: 07 Nov 2015.

Journal of Earthquake Engineering, 20:243–278, 2016

ISSN: 1363-2469 print / 1559-808X online
DOI: 10.1080/13632469.2015.1061465

Taylor & Francis
Taylor & Francis Group

Direct Displacement-Based Seismic Design of Eccentrically Braced Steel Frames

GERARD J. O'REILLY[1] and TIMOTHY J. SULLIVAN[2]

[1]ROSE Programme, UME School, IUSS Pavia, Pavia, Italy
[2]Department of Civil Engineering and Architecture, Università degli Studi di Pavia, Pavia, Italy

A series of eccentrically braced frames (EBF) are designed and subjected to nonlinear analyses to highlight ambiguities and differences in current seismic design provisions for EBF structures. This provides motivation to implement better guidance for the checking of local displacement demand considerations and move towards a displacement-based design approach. A recently proposed direct displacement-based design (DDBD) procedure for EBFs is then described and further developed in this article through the calibration of a spectral displacement reduction factors that relate the displacement of an inelastically responding structure to that of the equivalent linear representation used in the DDBD of EBFs. Such an expression is calibrated as part of this study using an experimentally validated numerical model also proposed here for the EBF links such that the actual hysteretic behavior of the links is well represented. The DDBD guidelines are applied to EBF systems from 1–15 stories in height and their performance is verified via nonlinear dynamic analyses using two different sets of design spectrum compatible ground motions. The results of the study indicate the robustness of the proposed DDBD method in limiting the interstory drifts to design limits for a variety of EBF systems with short links, thus demonstrating that the proposed DDBD method is an effective tool for seismic design of EBFs.

Keywords Eccentrically Braced Frame; Displacement-based Design; Numerical Modeling; Spectral Displacement Reduction Factor; Steel; Eurocode 8

1. Introduction

Investigations into the seismic behavior of eccentrically braced steel frames (EBFs) appear to have originated in Japan during the 1970's, where Tanabashi *et al.* [1974] performed a series of static tests on vertical Y-link configurations to examine the hysteretic properties of this eccentric configuration. Extensive experimental investigations into the behavior of EBF structures using horizontal links, such as that shown in Figure 1, were conducted at the University of California at Berkeley in the late 1970's/early 1980's [Roeder and Popov, 1977; Hjelmstad and Popov, 1983; Popov and Malley, 1983; Kasai and Popov, 1986; Engelhardt and Popov, 1989b], where numerous experiments were performed to determine the behavior of these links and the influence of stiffener detailing on their performance, and also more recently at the University of Texas during the 2000's [Arce, 2002; Galvez, 2004; Okazaki and Engelhardt, 2007; Ryu, 2005]. These tests formed the basis for the development of the EBF system, as these experimental campaigns demonstrated the stable

Received 22 November 2014; accepted 8 June 2015.
Address correspondence to Gerard J. O'Reilly, ROSE Programme, UME School, IUSS Pavia, Pavia, Italy. E-mail: gerard.oreilly@iusspavia.it
Color versions of one or more of the figures in the article can be found online at www.tandfonline.com/ueqe.

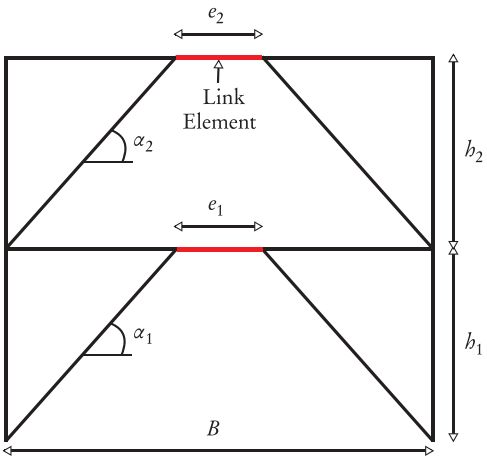

FIGURE 1 Typical layout of an EBF.

hysteretic behavior of ductile links. One aspect of the EBF that makes it particularly desirable as a ductile lateral load-resisting system is that it possesses an initial stiffness similar to a concentrically braced frame, which is generally seen to be beneficial in terms of limiting lateral displacements and story drift, but also having the energy dissipation capacity of a moment-resisting frame, where the stable hysteretic response of the links dissipate large amounts of energy in comparison to a similar concentrically braced frame configuration.

In comparison to other steel structures, such as moment-resisting frames and concentrically braced frames, reconnaissance information for EBFs is not widely available. However, a series of post-earthquake investigations have been conducted for a number of EBF structures subjected to the 2010 and 2011 Canterbury earthquakes in New Zealand, which reported on damage to both medium- and high-rise EBF building structures, as well as parking garages, subject to the two different earthquakes. Bruneau *et al.* [2010] notes that recently constructed buildings in the downtown Christchurch area, such as the 22-story Pacific Residential Tower, relied on EBFs as the lateral load resisting system. In general, these structures were reported as having performed very well with only minor flaking of the link element paint being reported, which led to these structures being green-tagged following the earthquake. Clifton *et al.* [2011] noted that estimates of peak shear strain demand were of the order of 0.03–0.04 in one structure, which is well below the NZS3404 [NZS 3404, 2007] limit of 0.08 if shear strain is taken to be equal to the link chord rotation, although this structure was noted to have been designed for a lower target ductility due to its height and plan dimensions [Bruneau *et al.*, 2010]. This was again the case for the 2011 event, as reported by Bruneau *et al.* [2011], which is an interesting point as both events were generally stronger than the design demand level specified by NZS3404.

Design codes such as Eurocode 8 [EN 1998-1:2004, 2004], New Zealand's NZS3404 [NZS 3404, 2007], Canada's CSA S16-09 [CSA S16-09, 2009], and the US AISC 341-10 [AISC 341-10, 2010] utilize the design philosophy often termed force-based design (FBD), which designs a structure for a set of reduced seismic forces depending on the structural system's ductility capacity by using either the equivalent lateral force or modal response spectrum methods of analysis. However, as discussed in Priestley [1993] and Priestley *et al.* [2007], this design approach possesses a number of fundamental shortcomings, such as the use of unique force-reduction factors for structural systems regardless of the structural configuration or actual ductility capacity. Some codes have been modified to incorporate displacement-based design considerations for EBF link deformations, although it will be

shown shortly that in the case of EBF design provisions in Eurocode 8 (EC8), there appears to be a need for improved consideration of displacements and deformations within the design process. Other energy-based methods have been proposed by Goel *et al.* [2009] and Sullivan [2011] which design the structure based on relating the input energy of the seismic action to the dissipated energy of the actual structure's plastic mechanism.

Some issues with current code design approaches particular to EBF systems are identified in the next section to provide motivation for the development of DDBD for such systems, where, by examining a series of case study SDOF EBFS designed using both European and U.S. design code approaches, it is shown that comprehensive guidance ought to be given in the determination of link demands for EC8, while both U.S. and European provisions show large variability in actual link demand to capacity ratios at the expected drift level. In light of this, a clarification has been proposed for EC8 to improve the estimation of link demands through the use of elastic analysis, as is normally carried in current code design. While it is shown how current methods can be modified and improved, it is also shown how the same issues of variability in actual design capacity do not exist with DDBD and resulting designs are more consistent in establishing link deformation demands, which is the main focus of this article. However, the DDBD procedure for EBFs recently proposed by Sullivan [2013a] has not been extensively verified through detailed experimental calibration and numerical validation. This article therefore aims to refine the existing DDBD approach for EBFs by first proposing a newly calibrated numerical to accurately represent the hysteretic behavior of the EBF system. Through this model, spectral displacement reduction factors are developed in support of DDBD and a series of case study structures are designed and analysed using nonlinear time history analysis to verify the performance of the proposed DDBD method. The work examines EBF structures with short links only, even though many of the observations would be relevant to EBFs with long links as well.

2. Review of Current Design Code Approaches

This section reviews the current design approach to the seismic design of EBF structures and provides guidance on the use of elastic analysis to predict inelastic demands in the link element. This is done through examination of a series of single-story EBF structures that are designed using both European and U.S. code provisions. The expected inelastic deformation capacity is determined via pushover analyses and compared to available capacity as predicted in order to highlight variability obtained using code approaches. This analysis and discussion also provides the motivation for an alternative DDBD approach for the seismic design of EBFs.

2.1. Case Study Design of SDOF EBFs to EC8 and AISC 341-10

Table 1 shows a total of 16 different case study EBF structures designed to both European [EN 1998-1:2004, 2004] and U.S. seismic design code provisions [ASCE 7-10, 2010; AISC 341-10, 2010]. The case study structures consist of a single-story EBF with varying link length (e), bay width (B), story height (h), steel grade (f_y) and seismic mass (m). Each structure is designed to the soil type C design spectrum discussed further in Section 4.1.2, which has an equivalent peak ground acceleration on rock of 0.4 g. It should be noted that this design spectrum is as per European seismic design provisions and is used for the calculation of seismic design forces for both EC8 and AISC design cases in order to maintain consistency. For each case, a short EBF link structure is assumed and an importance factor of 1.0 is used for both design codes. A behavior factor (q) and displacement amplification factor (q_d) of 6.0 are used for European designs, as per EN 1998-1:2004 [2004], and

TABLE 1 Case study designs according to EC8 and AISC 341-10

						Eurocode 8			AISC 341-10		
Case	e [m]	B [m]	h [m]	f_y [MPa]	m [t]	Link/Beam	Brace	Column	Link/Beam	Brace	Column
1	0.4	7	3.2	275	150	HE140B	HE140B	HE100B	HE120B	HE140B	HE100B
2	0.6	7	3.2	275	150	HE140B	HE140B	HE100B	HE140B	HE140B	HE100B
3	0.8	7	3.2	275	300	HE200B	HE160B	HE120B	HE180B	HE160B	HE120B
4	1.2	7	3.2	275	300	HE280AA	HE180B	HE120B	HE260AA	HE160B	HE120B
5	0.4	7	3.2	460	250	HE140B	HE160B	HE120B	HE160B	HE180B	HE120B
6	0.6	7	3.2	460	250	HE160A	HE160B	HE120B	HE160B	HE160B	HE120B
7	0.8	7	3.2	460	500	HE200B	HE180B	HE140B	HE200B	HE200B	HE160B
8	1.2	7	3.2	460	500	HE260AA	HE200B	HE140B	HE260AA	HE200B	HE140B
9	0.4	5	3.2	460	250	HE160B	HE140B	HE120B	HE180A	HE140B	HE120B
10	0.6	5	3.2	460	250	HE160B	HE140B	HE120B	HE180A	HE140B	HE120B
11	0.8	5	3.2	460	500	HE240B	HE160B	HE160B	HE220B	HE160B	HE140B
12	1.2	5	3.2	460	500	HE240B	HE160B	HE160B	HE220B	HE160B	HE140B
13	0.4	5	4	275	150	HE180B	HE120B	HE140B	HE160B	HE120B	HE120B
14	0.6	5	4	275	150	HE180B	HE120B	HE140B	HE160B	HE140B	HE120B
15	0.6	5	4	275	300	HE280B	HE160B	HE160B	HE240B	HE140B	HE140B
16	1.2	5	4	275	300	HE280B	HE160B	HE160B	HE240B	HE140B	HE140B

a force reduction (R) and displacement behavior factor (C_d) pair of 8 and 4 are used for U.S. designs, as per AISC 341-10 [2010], respectively. For both design code approaches, the design base shear is determined and the link members designed in accordance with EC8 and AISC for European and U.S. designs, respectively. The surrounding elements such as the columns and brace members are designed in accordance with the relevant capacity design and member capacity checks for Eurocode 3 [EN 1993-1-1:2005, 2005] and AISC 360-10 [AISC 360-10, 2010] standards. For each of the structures designed, the lateral displacement was determined through an elastic analysis of the trialled section sizes and subsequently amplified by the relevant displacement amplification/behavior factor for each design code. In the event of the link deformation check indicating a deformation capacity exceedance at the amplified elastic story drift, the trial link section size was modified to increase strength and stiffness in the EBF. This iteration was necessary for a total of four cases for AISC designs, where a satisfactory design was established after typically two or three extra trials. In addition, the initial period was determined via eigenvalue analysis of the trial design and used in the subsequent iterations of design in place of the initial period estimate expressions provided by the design codes.

The chord rotation demand determination is somewhat a source of discrepancy between design codes, as EC8 states (cl. 4.3.4) that "the displacements induced by the seismic design action shall be calculated on the basis of the elastic deformations of the structural system" and that the link rotation can be found (cl. 6.8.2(10) and 6.6.4(3)) as the total link relative deflection at midspan divided by half the link length, while the commentary provided in AISC 341-10 states that the link demand should be computed as a function of the plastic interstory drift. The amplification of elastic deformation demands for EC8 and the use of plastic story drift for AISC 341-10 are utilized here in the estimation of link demands, respectively, in order to highlight an important difference. The demand to capacity ratio of the link plastic chord rotation is then determined for each approach, where the design plastic chord rotation capacity is taken as 0.08 rad for short links, as per both design codes. These ratios are plotted for each case in Figure 4 as the amplified elastic

demand case, where it can be seen that all of the ratios are below unity, indicating that none of the designs are expected to exceed the link capacity, while the AISC approach of using plastic drift shows a marked difference in demand to capacity ratio estimation when compared to the amplified elastic link demand approach used in EC8.

2.2. Pushover Analysis of Case Study Structures

In order to perform a pushover analysis on the case study structures, a numerical model that can accurately represent the nonlinear behavior of short link EBFs needs to be established. This section first presents such a model followed by the actual pushover analysis of the case study structures in order to evaluate their deformation capacity. This modeling will also be used for the nonlinear time history analyses carried out later in this article.

2.2.1. Link Model Overview. In this work, a force-based fiber element model is developed in OpenSees [McKenna *et al.*, 2000]. To this extent, it is proposed that the behavior of short links employed in EBFs can be represented numerically by using a force-based fiber-element to model axial and flexural behavior, along with an uncoupled shear hysteretic behavior to account for the flexibility and nonlinearity due to shear response in the link, as recommended by Malakoutian *et al.* [2013], but with the exception that the hysteresis rule used for the shear behavior is changed to account for isotropic hardening and the plateau of the maximum shear force in the element. While the approach of Malakoutian *et al.* [2013] was shown to work well for a number of specimens, it does not seem appropriate to ignore the link's isotropic hardening behavior, as is evident when consulting some of the observations made in the experimental tests discussed in the literature [Okazaki *et al.*, 2009; Engelhardt and Popov, 1989a; Kasai and Popov, 1986; Mansour, 2010; Popov *et al.*, 1987; Hjelmstad and Popov, 1983], where the hysteretic cycles were seen to "grow" with increasing deformation amplitude. The approach proposed here is to therefore use a different hysteresis rule and calibrate its parameters to give a behavior that is more representative of that observed in previous experimental tests. The hysteretic rule adopted for the EBF shear hinge is the Giuffre Menegotto-Pinto hysteresis rule, and a complete description of the relevant terms can be found in the OpenSees command manual [McKenna *et al.*, 2000]. The yield force input to the material model is the link yield force (V_y), with an initial stiffness of GA_v, where G is the steel shear modulus and A_v the shear area of the link, along with a post yield hardening ratio of 0.001. The elastic-plastic transition parameters ($R0$, $cR1$ and $cR2$) are taken as 20, 0.925, and 0.01, respectively, and the isotropic hardening parameters ($a1$, $a2$, $a3$, and $a4$) are taken as 0.02, 1, 0.02, and 1, respectively. This material is then aggregated into a fiber-element using the section aggregator tool within OpenSees.

2.2.2. Validation with Experimental Results. Using the link modeling parameters outlined in Section 2.2.1, results obtained using the proposed modeling approach are compared with existing experimental data to validate its performance as a modeling approach for short link EBFs. Experimental test results from Mansour [2010] and Okazaki *et al.* [2009] have been digitized and compared with the proposed model. Details of these test specimens are given in Table 2, where all tests adopted the EBF link loading protocol specified in the 2005 version of AISC 341 [AISC 341-05, 2005].

A comparison of the hysteretic responses of the links observed for each of the specimens listed in Table 2 and the proposed model is shown in Figure 2, and it can be seen that the proposed model and experimental results match very well. This is highlighted in the isotropic hardening of the links between cycles and the good representation of the stiffness transitions between the elastic and inelastic branches of behavior. As such, it is concluded

TABLE 2 Test specimen details for links used in model validation

Reference	Specimen ID	Section Size	Link Length [mm]	Loading Protocol
Mansour [2010]	UT3A	W360 × 101	900	AISC 341-05 [2005]
Mansour [2010]	UT3B	W360 × 101	900	AISC 341-05 [2005]
Okazaki *et al.* [2009]	AISC-2	W18 × 40	980	AISC 341-05 [2005]
Okazaki *et al.* [2009]	AISC-6	W10 × 68	980	AISC 341-05 [2005]

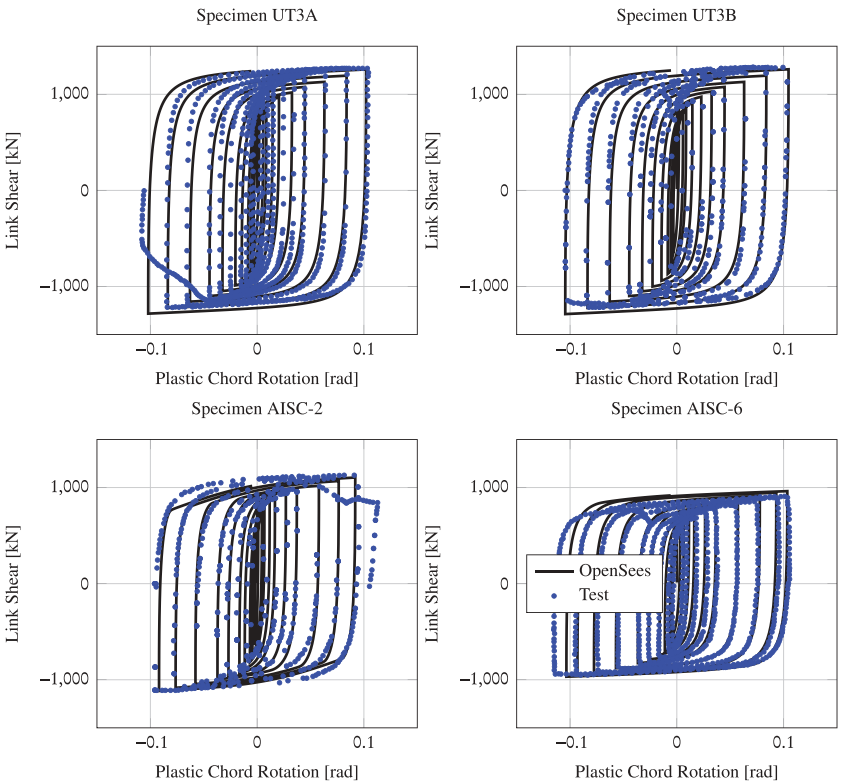

FIGURE 2 Validation of numerical model with experimental data.

that the modeling parameters proposed here match actual experimental behavior very well and are recommended for the fiber-element modeling of short link EBF structures. Note that the model is proposed for modeling of links with stable hysteresis and intermediate web stiffener detailing as per Eurocode, AISC, and CSA requirements.

2.2.3. Single-Story Model. The short link fiber-element modeling approach is now expanded into a single-story EBF model to consider the behavior of an entire story of an EBF structure, not just the principal component of its nonlinear behavior. Figure 3 shows the proposed model that includes the validated shear link model in addition to an arrangement of beams and columns to represent a single story of an EBF structure. Beam elements are assumed to have pinned connections to the outer columns, as are the brace members. It is acknowledged that connections between braces and the underside of the beam members

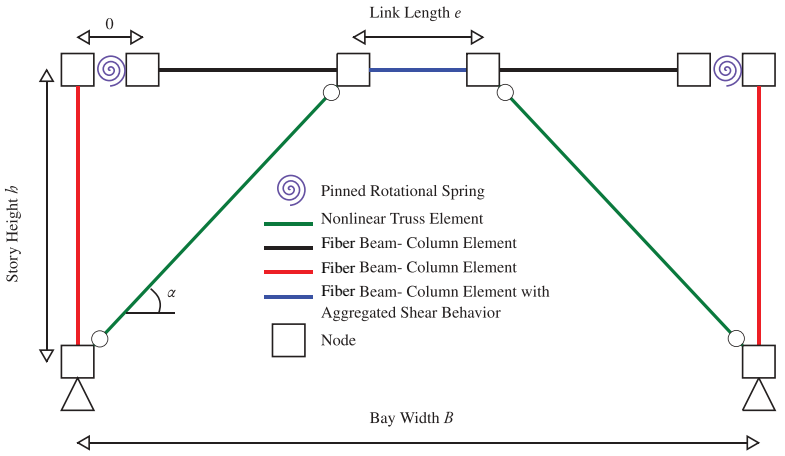

FIGURE 3 Single-story model for EBFs.

may consist of welded connections with a stiffened beam web to transfer large shear forces from the braces through to the link, which has been demonstrated to be very important for the performance of EBF systems through the observations of Kanvinde *et al.* [2014] after the performance of an EBF during the 2011 Canterbury earthquake. However, the moments transferred through to the braces are generally quite low in comparison to the moments transferred to the outer beams and the governing forces acting through the braces are axial forces [Nascimbene *et al.*, 2012]. It is therefore deemed reasonable to idealize the brace to beam connection as a pinned connection and assume the moments developed in the links are transferred to the outer beams only, and this has therefore been the adopted approach for the model shown in Figure 3.

2.2.4. Pushover Results. Using the numerical model proposed in Section 2.2.3, an inelastic pushover analysis is performed on each of the designs listed in Table 1 to the expected interstory drift demand, as determined from the code procedure. The resulting demand to capacity ratio of the actual link plastic chord rotations at this expected drift are then computed and plotted in Figure 4. As is immediately obvious from Figure 4, many of the EC8 design solutions exceed the link plastic chord rotation capacity at the expected drift and the amplified elastic link demand estimates are consistently underestimating the actual

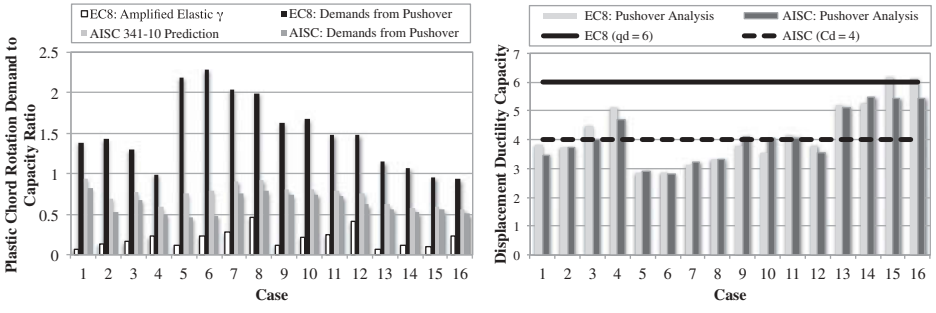

(a) Demand to capacity ratios. (b) Displacement ductility capacities.

FIGURE 4 Evaluation of European and U.S. design solutions.

link demands, whereas the AISC designs are closer to a demand to capacity ratio of unity. Note that in order to arrive at the final AISC solutions, iteration was required in cases where the initial design solution (obtained using a force reduction factor of 8) was found to lead to excessive plastic chord rotation demands. This illustrates how the displacement-based considerations adopted in AISC 341-10 can effectively limit the plastic chord rotation demands to within an acceptable level. Also shown in Figure 4b are the displacement ductility capacities, obtained by pushing each of the EBF case study models to a plastic chord rotation of 0.08 rad and dividing the observed story displacement by the yield displacement of the EBF. As such, Figure 4b clearly illustrates that the use of a single behavior (or force reduction) factor does not result in consistent levels of ductility capacity for all EBF systems, while AISC does a reasonable job compared to EC8, which tends to expect much more ductility at the design displacement than is actually available. This variability in design demand to actual capacity highlights one of the principal shortcomings of current code-based seismic design discussed in Priestley *et al.* [2007], where the use of unique force reduction/displacement amplification factors is argued to be an illogical approach that does not consider geometrical or material property variations of the structure.

2.3. Improved Estimation of Link Plastic Deformation Demands in FBD

To better understand the results presented in the previous section and identify a means of improving the EC8 approach, note that the yield drift of a given story of an EBF structure has three main components [Sullivan, 2013a]: (i) flexibility of the link and beams (ii) flexibility of the brace elements and (iii) drift due to axial compression of the columns beneath the story of interest. The drift contribution from each of these three components is determined here for three separate EBF structures to illustrate how each contributes to the interstory drift of a story within an EBF structure. The three example structures are taken from Sullivan [2013a], with the modeling procedure described in Section 2.2.1 used to model the structures. A pushover analysis up to a displacement corresponding to 1% interstory drift of each structure is performed and the individual components of story drift are illustrated in Figure 5.

As previously mentioned, EC8 allows the computation of deformation demands in the inelastic range of response from elastic analysis assuming that the ratio between the contributions of the link, brace, and column deformation are preserved at all displacements through the amplification of elastic demands. It is clear from Figure 5 that this is not the case, with the contribution of the brace and column deformations effectively plateauing after story yield with the increasing drift contribution coming from the deformation of the link. This means that the actual inelastic link demand is higher that what is determined by amplification of elastic deformation demand, which explains the observations in Figure 4, where the actual link demands observed from pushover analyses were of much higher magnitude than those estimated from elastic deformation amplification. This has been noted elsewhere [Kusyilmaz and Topkaya, 2014] as somewhat of a grey area in code specifications with only the Commentary of AISC 341-10 providing some prescriptive guidance and EC8 not providing any explicit statement as to how to determine these demands.

A simple expression can be derived to aid the calculation of actual link demand when using EC8. This relation, which is also described at least in principle in the Commentary of AISC 341-10, assumes that the contribution of the braces and columns to the interstory drift remains constant upon yielding of the link element and the actual link plastic chord rotation demand for a story i is given as:

$$\gamma_{p,i} = \frac{d_e B_i}{e_i h_i}(\mu_i - 1) = \frac{B_i\left(\theta_{max,i} - \theta_{y,i}\right)}{e_i}, \tag{1}$$

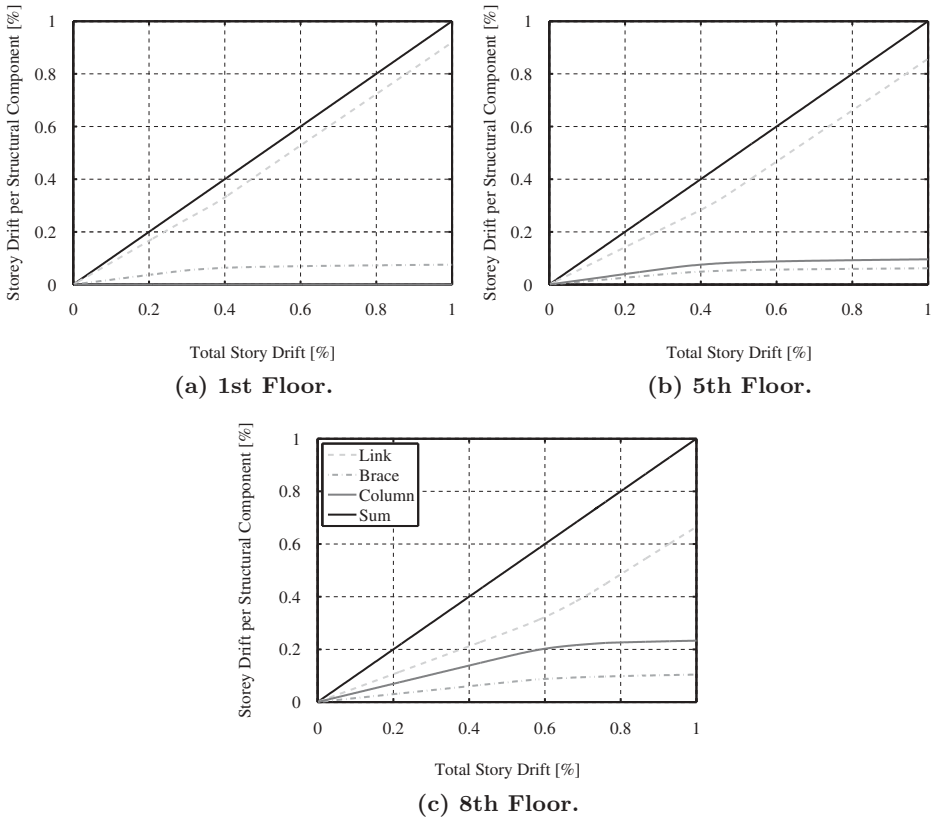

FIGURE 5 Interstory drift contribution.

where d_e is the elastic relative story displacement of a story i determined from elastic analysis, μ_i is the story ductility defined as the peak story drift $\left(\theta_{max,i}\right)$ divided by the story yield drift $\left(\theta_{y,i}\right)$. Alternatively, the displacement amplification factors provided by design codes (C_d or q_d) may be used in the absence of a ductility term (μ), even though this approach may be inaccurate for cases where one has links of different length in different bays of the same story or different values of overstrength over the height of the structure. Note that the expression on the right in Equation (1) would be useful when non-uniform ductility demands are expected over the height of the structure. The discrepancy between amplified elastic link demands and actual link demands increases linearly with ductility, which is of great concern to the bottom stories of MDOF EBF structures, which tend to be the critical story with high ductility demand compared to the upper stories. Thus, if the link chord rotation demand at the design level is currently being underestimated through the lack of explicit guidance in EC8, the probability of mechanisms such as soft-story collapse increases as a result of the increased risk of link fracture due to excessive link chord rotation demands. Figure 6 demonstrates that by using Equation (1), the estimate of demand to capacity ratios greatly improves for the case of EC8, whereas AISC provisions already outline such a method in the commentary. The slight overestimation by Equation (1) in Figure 6 is attributed to the simplifying assumption of a purely plastic mechanism forming in the link without strain hardening. The results of Figure 6 illustrate that if the EC8 design procedure were to adopt Equation 1 to check plastic chord rotation demands, it would prompt changes to the vast majority of the initial design solutions

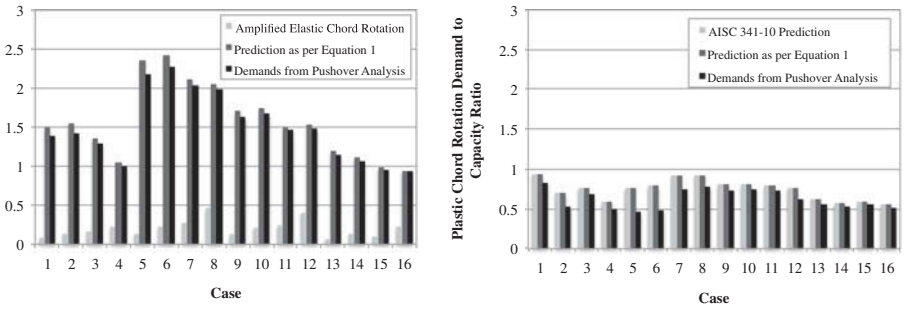

(a) Eurocode 8.

(b) AISC 341-10.

FIGURE 6 Demand to capacity ratio of link plastic chord rotation.

presented earlier in Table 1, as these would be found to fail the link deformation demand limits. This highlights the urgent need to make changes to the current EC8 prescriptions. Note that once this issue is addressed, the best means of changing the structure to reduce excessive chord rotation demands may still not be clear and the designer must go through a series of revisions to satisfy both force and displacement requirements; it was found that the AISC cases in Section 2.1 typically took 2 or 3 iterations to complete. Such an exercise can be quite time consuming and in addition to design calculations, the designer must also have prepared an analytical model of the structure to determine the elastic displacements and deformation of the structure. This is one of the main benefits of moving towards the displacement-based design approach presented in the following section, where the focus is to control link deformations rather than forces and a design solution can be obtained in a single step rather than a series of iterations requiring analytical software.

3. Direct Displacement-Based Design of Eccentrically Braced Frames

The previous section has demonstrated that there is some discrepancy with current EC8 design guidelines for EBF systems with different procedures for determining expected design deformations and considerable effort required to give a satisfactory design. Such issues motivate the development of alternative seismic design approach and in this section, the DDBD procedure of Priestley *et al.* [2007] and extended by Sullivan [2013a] to EBFs is reviewed and refined.

3.1. Overview of DDBD

The DDBD methodology [Priestley *et al.*, 2007] allows for the design of a structure to specified target displacements and thus, a specific performance level that can be related to chord rotation and interstory drift limits. The key steps of DDBD are summarised in Figure 7, where an SDOF system is used to represent an MDOF system at maximum displacement in its first fundamental mode of response (Figure 7a), which for the specific case of EBFs will be discussed in Section 3.5.1. Figure 7b shows the SDOF representation of the structure as an equivalent linear system with secant stiffness to the design displacement. To account for the effects of energy dissipation and nonlinear response, the equivalent linear SDOF is attributed an equivalent viscous damping coefficient (as per Priestley *et al.*, 2007) or a displacement reduction factor (used here) as a function of the level of ductility demand, as shown in Figure 7c and discussed further in Section 3.2.2. For the case of EBF structures,

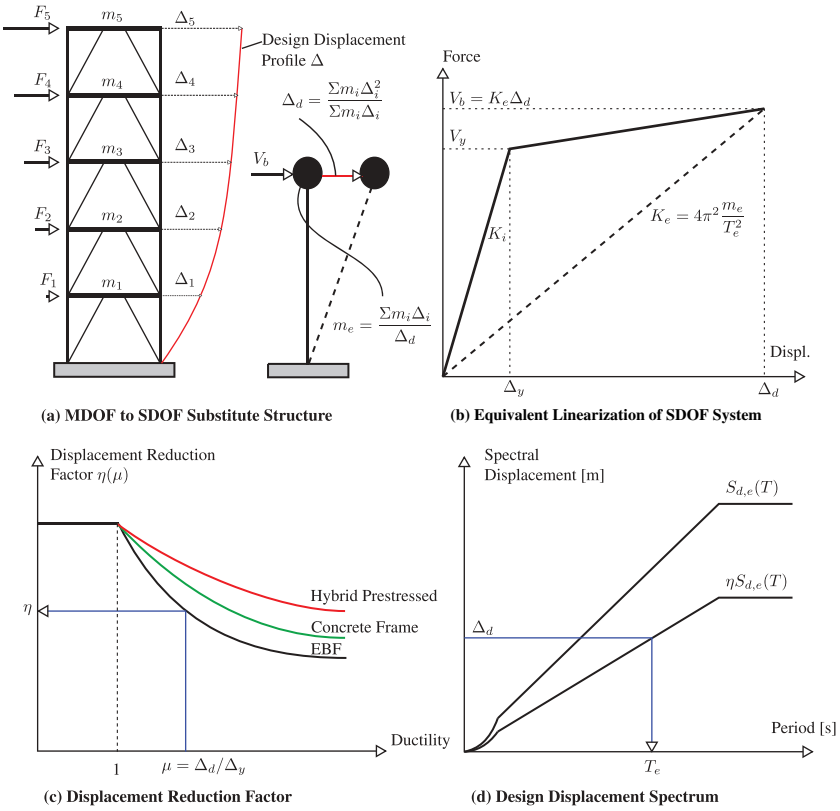

FIGURE 7 Fundamental aspects of the DDBD procedure (after Priestley *et al.*, 2007).

a DRF specific to EBFs is developed in Section 3.3 as a part of this article. The target displacement ductility is a function of the system yield displacement and target displacement. The yield displacement can be typically found from geometry and material strain definitions, whereas the target displacement for EBFs is determined from plastic chord rotation or interstory drift limits, which means that the structure's displacements are a key definition of the design process that can be adjusted to control certain limits states. As shown in Figure 7d, the design displacement is then used in conjunction with the DRF to enter the DRF-reduced spectral displacement response spectrum in order to determine the required effective period (T_e) of the equivalent linear system. Using the effective period, the effective stiffness, K_e of the SDOF system at the target displacement is determined from the expression given in Figure 7b, where m_e is the effective mass. The product of effective stiffness and the design displacement, Δ_d, provides the design base shear V_b as per Figure 7b. This is therefore a direct method that does not require iterations of initial period or elastic analysis to determine design displacement demand and a complete design can be obtained on one single spreadsheet.

To extend the DDBD approach to MDOF structures, the substitute structure concept of Gulkan and Sozen [1974] and Shibata and Sozen [1976] is used to identify the SDOF properties of a MDOF system assuming a certain displaced shape at maximum response. This is used to find the design target displacement, Δ_d, of the structure and its effective mass, m_e that are used in the DDBD process outlined previously. The expressions for these terms are given in Figure 7a where n is the number stories in the structure, Δ_i comes from

the design displacement profile for the structure (see Section 3.5.1) and H_i is the story elevation, as outlined in Priestley *et al.* [2007].

3.2. DDBD of SDOF EBF Structures

3.2.1. EBF Story Displacement Capacity. The first step in DDBD of SDOF EBFs is the determination of the design displacement and ductility as a function of the story drift through the expressions:

$$\Delta_d = \theta_d h \tag{2}$$

$$\mu = \frac{\theta_d}{\theta_y}, \tag{3}$$

where Δ_d is the design displacement, h is the interstory height at story i and the design drift (θ_d) is determined as the drift capacity $(\theta_{c,i})$. The drift capacity of a given story in an EBF is computed as the sum of the yield $(\theta_{y,i})$ and plastic $(\theta_{p,i})$ story drift components. As mentioned previously, the story yield drift of an EBF structure is principally composed of deformations of three components: (i) link (and beam) bending and shear deformation $(\theta_{link,i})$, (ii) brace axial deformation $(\theta_{br,i})$, and (iii) column axial deformation $(\theta_{col,i})$. These individual contributions to the yield drift of an EBF are discussed in detail in Sullivan [2013a] and the final expressions describing each contribution are noted here for brevity and completeness as:

$$\begin{aligned}\theta_{y,i} &= \theta_{link,i} + \theta_{br,i} + \theta_{col,i} \\ &= \frac{f_y A_{v,i} e_i}{\sqrt{3}\,(B - e_i)} \left(\frac{e_i\,(B - e_i)}{12 E I_{zz,i}} + \frac{1}{G A_{v,i}} \right) + \frac{2 k_{br,i} \epsilon_y}{\sin(2\alpha_i)} + \frac{2 k_{col,i-1} \epsilon_y H_{i-1}}{B},\end{aligned} \tag{4}$$

where the general notation is as illustrated in Figure 1, with $I_{zz,i}$ representing the second moment of area of the beam about the major axis, E and G are the elastic and shear moduli of steel, respectively, $A_{v,i}$ is the shear area of the link element, f_y is the steel yield strength, ϵ_y is the steel yield strain, α is the brace angle and $k_{br,i}$ represents the ratio of the actual strain in the brace to the yield strain, which can be computed as the axial force ratio in the brace, as follows:

$$k_{br,i} = \frac{N_{Ed,br,i}}{N_{c,Rd,br,i}}, \tag{5}$$

where the terms $N_{Ed,br}$ represents the DDBD first mode axial force on the brace member and not the final capacity design axial force since the expected brace strain for DDBD is required here. The term $N_{c,Rd,br}$ represents the compressive axial capacity (Af_y) of the brace section, not to be confused with the member buckling capacity.

The right most term in Equation (4) includes a story drift term component due to column axial deformations. For SDOF EBF systems, this term can be taken as zero. For MDOF systems, it should be computed noting that the term H_{i-1} is the elevation of the floor below the one being considered and $k_{col,i-1}$ represents the average expected column axial force to the yield of these column sections, similar to the k_{br} ratio shown above. As there can be many stories below the story i being considered, there are many ratios of expected

to capacity axial load ratios, which were found to typically vary from 0.3–0.4. The average ratio can therefore used in Equation (4), which is calculated by:

$$k_{col,i-1} = \frac{1}{i-1}\sum_{j=1}^{i-1}\frac{N_{Ed,col,j}}{N_{c,Rd,col,j}} \tag{6}$$

Note that the k_{br} and k_{col} ratios in Equations (5) and (6) are iterative and may appear somewhat difficult to establish but are actually completely within the designer's control. This is because the designer chooses the final column and brace sections and therefore, if desired, could select final column and brace sections that respect the k_{br} and k_{col} values adopted during DDBD, provided that the final member sizes are also checked for capacity design actions. Since some iteration may result during the determination of both k_{br} and k_{col}, acceptable tolerances are suggested to be of the order of 0.01 which is typically achieved quite quickly after just a few iterations. This was demonstrated through example application in the Appendix of Sullivan [2013a], where just two iterations were required. However, should a design spreadsheet be prepared, the initial values for k_{br} and k_{col} can be directly linked to the computed values from the selected braces and column section sizes, meaning that the spreadsheet automatically updates itself for instantaneous convergence.

As the total drift capacity of an EBF is a combination of the yield drift plus the plastic drift capacity, it is given by:

$$\begin{aligned}\theta_{c,i} &= \theta_{y,i} + \theta_{p,i} \\ &= \frac{f_y A_{v,i} e_i}{\sqrt{3}\,(B-e_i)}\left(\frac{e_i\,(B-e_i)}{12EI_{zz,i}} + \frac{1}{GA_{v,i}}\right) + \frac{2k_{br,i}\epsilon_y}{\sin(2\alpha_i)} + \frac{2k_{col,i-1}\epsilon_y H_{i-1}}{B} + \frac{e_i\gamma_p}{B},\end{aligned} \tag{7}$$

where γ_p is the link plastic chord rotation capacity, for which current code defined limits for design are given as 0.08 rad and an ultimate limit of 0.10 rad is specified for both EC8 and AISC 341-10.

3.2.2. Equivalent Viscous Damping and Spectral Displacement Reduction Factors. In addition to the design displacement and ductility, one requires knowledge of the equivalent viscous damping or displacement reduction factor (DRF) for the DDBD of EBFs, which is illustrated in Figure 7c to be directly related to ductility (μ). Section 3.3 discusses the development of a DRF expression for EBF systems, which is given here as:

$$\eta = \begin{cases} 1.0 & \text{for} \quad \mu \le 1 \\ 2.16\exp(-1.6\mu) + 0.56\exp(0.01\mu) & \text{for} \quad \mu > 1 \end{cases}. \tag{8}$$

3.2.3. Effective Period and Base Shear. The next step of the EBF design is to compute the effective period and design base shear. This can be done using the ductility dependent DRF determined from Equation (8) to reduce the design spectrum, as outlined in Figure 7d. Using this reduced design spectrum, the required effective period (T_e) is obtained by entering the spectrum with the target design displacement (Δ_d) and finding the corresponding period on the reduced spectrum, as illustrated in Figure 7d. As per Figure 7b, the required effective stiffness for the equivalent linear SDOF system is given by:

$$K_e = \frac{4\pi^2 m_e}{T_e^2} \tag{9}$$

and the base shear is then determined, with the inclusion of additional capacity to account for P-Delta effects, as follows:

$$V_b = K_e \Delta_d + C\frac{\sum_{i=1}^{n} P_i \Delta_i}{H_e} \quad C = \begin{cases} 1 & \text{for } \frac{m_e g}{K_e H_e} \geq 0.05 \\ 0 & \text{for } \frac{m_e g}{K_e H_e} < 0.05 \end{cases}, \tag{10}$$

where P_i represents the seismic weight at a given floor i and C is a P-Delta effect coefficient, whose limits are proposed by Priestley *et al.* [2007] and Sullivan *et al.* [2012] for steel structures as shown.

3.2.4. Link Member Sizing. Using the design base shear, the design shear forces ($V_{Ed,link,i}$) on the link elements can be determined from equilibrium, which for a given story (also in MDOF systems) is then:

$$V_{Ed,link,i} = \frac{V_i h_i}{B}. \tag{11}$$

In order to size sections for these links, the actual strength of the link should be determined at the design plastic chord rotation. This requires knowledge of the strain-hardening provided by the section at the design level of deformation. Using the hysteretic model proposed for EBFs in Section 2.2.1, this expected overstrength is in the region of 1.25 and as such is proposed. It is acknowledged that this value of 1.25 is somewhat smaller than the values discussed in the literature [Della Corte *et al.*, 2013; Mohebkhah and Chegeni, 2014], but it is envisaged that these values represent the best comparison to the value obtained from the numerical model that is used to evaluate the structure. The actual strength increase with deformation may, however, also be affected by slab resistance (not modeled) and therefore the value indicated in Equation (12) may need to be revised in the future should significant slab interaction be anticipated. Considering the above, the resistance offered by the link ($V_{Rd,link,i}$) at the design drift level is given as:

$$V_{Rd,link,i} = \begin{cases} \frac{\theta_i}{\theta_{y,i}} V_{y,link.i} & \text{for} \quad \mu \leq 1 \\ \left(1 + 0.25\frac{\gamma_{p,i}}{\gamma_p}\right) V_{y,link,i} & \text{for} \quad \mu > 1 \end{cases}, \tag{12}$$

where $\gamma_{p,i}$ is the plastic chord rotation demand for level i and γ_p is the design plastic chord rotation capacity, typically taken as 0.08 rad as outlined previously.

In order to provide a uniform distribution of design strength in each story of MDOF systems, the overstrength of the EBF system, defined as the ratio of the actual resistance provided to the design force, is limited to avoid providing excessive overstrength in certain stories and hence a concentration of damage in the adjacent stories. EC8 specifies that the additional overstrength of the link members (Ω) be no more than 1.25 times the required design strength to avoid such issues, which is adopted here.

3.2.5. Capacity Design. The final step in the seismic design process is to confirm the sizes of the brace and column sections and any other elements or connections not intended to yield during seismic response through the application of capacity design rules. In order to do this, the actual forces generated by the yielding link elements needs to be properly identified and amplified so that the sizing of the capacity design protected elements is sufficient to ensure they remain elastic during seismic response. Amplification factors for brace and columns vary between 1.375 and 1.5 times the expected force generated by the

link members [EN 1998-1:2004, 2004; CSA S16-09, 2009; AISC 341-10, 2010; NZS 3404, 2007], where a value of 1.5 times the force developed in the link $\left(V_{Rd,link,i}\right)$ was proposed in Sullivan [2013a] for the DDBD of EBFs and this same value is adopted here for simplicity. Once amplified actions have been found, standard code expressions for member resistances can be applied to verify the section resistances.

3.3. Development of a Spectral Displacement Reduction Factor for EBFs

The concept of equivalent viscous damping (EVD) was first introduced by Jacobsen [1930], where the hysteretic damping associated with the energy dissipation in nonlinear systems was related to the area enclosed by the hysteretic loop. Jacobsen [1930] proposed that this EVD term could be equated to the energy absorbed by the system during a cycle of steady-state harmonic response. This assumption of steady-state response was subsequently shown by Dwairi *et al.* [2007] to be an unrealistic assumption for systems subjected to earthquake ground motions. Given this limitation with the classical EVD definition, Grant *et al.* [2005], Dwairi *et al.* [2007] and Pennucci *et al.* [2011] calibrated EVD expressions to a variety of hysteresis rules that match results obtained using nonlinear time history (NLTH) analyses. This EVD was a combination of both the elastic damping term, typically taken as 5%, and the hysteretic damping resulting from hysteretic energy dissipation. This EVD term was then used in conjunction with a damping-dependent displacement scaling factor (DSF) to relate the design displacements with and effective period for the substitute structure. The damping dependent DSF expression suggested by Priestley *et al.* [2007] for use in DDBD is that found in the previous 1998 version of the Eurocode, as this was found to provide the best inelastic displacement estimates when used together with the EVD expressions developed by Grant *et al.* [2005] and Dwairi *et al.* [2007].

More recent research by Pennucci *et al.* [2011] has shown that the use of separate DSF and EVD expressions results in a sensitivity as to the characteristics of the ground motions used to calibrate the EVD expression. Since the EVD expressions outlined in Priestley *et al.* [2007] are a function of ductility and the DSF is a function of EVD, Pennucci *et al.* [2011] proposed that the DSF be related directly to the ductility, instead of calibrating an intermediate EVD term. Pennucci *et al.* [2011] subsequently found that by relating a displacement reduction factor (DRF) directly to the ductility, the expression was relatively insensitive to the type of ground motions used, as was not the case with EVD expressions. Pennucci *et al.* [2011] thus proposed a revised set of DRFs for a series of hysteretic types that relate the DRF directly to the ductility. Three DRF curves are shown in Figure 7c for hybrid prestressed and concrete frames, for which expressions were calibrated by Pennucci *et al.* [2011], and for EBF systems for which no expression has been explicitly proposed to date. However, since a hysteretic model for short EBF links has been proposed in Section 2.2.1, this section presents the calibration of a new expression for short link EBFs based on this experimentally calibrated numerical model.

3.3.1. Proposed Methodology. In order to calibrate a DRF for an EBF system characterised by the numerical modeling parameters outlined in Section 2.2.1, a number of NLTH analyses are carried out on a series of SDOF oscillators. This is done to compute the maximum displacement of a nonlinear SDOF system and relate this to the maximum displacement obtained using an equivalent linear SDOF system using an appropriate DRF. By assuming two initial sets of parameters, initial period (T_i) and force reduction factor (R), the properties to be supplied to the hysteretic model described in Section 2.2.1 can be determined, where the force reduction factor (R) represents the ratio between the inelastic yield force of the SDOF oscillator and the elastic force associated with the elastic spectra

of the ground motion. This way, when the actual inelastic response of the SDOF oscillator is determined for a given ground motion, the corresponding ratio of elastic to inelastic displacement is determined. The variation of both initial periods and force reduction factors lead to a data set with a range of effective periods (T_e) and ductility demands (μ), defined at the absolute maximum response of the SDOF oscillator, which are of principle interest in DDBD. Since early work on the calibration of EVD expressions by Grant *et al.* [2005] showed that the EVD of a hysteresis rule can be sensitive to the effective period of the oscillator, this needs to be considered in this calibration. The period dependency of the EVD expressions calibrated by Grant *et al.* [2005] showed that for effective periods greater than 1 s, this dependency is relatively insignificant and could be ignored for practical design purposes since effective periods in DDBD tend to be longer than 1 s. Its influence was again considered in this calibration work, described in O'Reilly and Sullivan [2015], and it was concluded that its influence could be ignored, as per previous recommendations by Grant *et al.* [2005].

The calibration procedure adopted here is outlined in Figure 8, where each combination of initial period, force reduction factor, and ground motion record leads to a single data point on the plot of DRF vs. ductility. The initial parameters to be input into the hysteretic model are first computed and the dynamic analysis is run for the combination of initial period, force reduction factor and individual ground motion to give the actual displacement for the nonlinear SDOF system, Δ_a. From this, the effective period to the actual displacement is computed and the spectral displacement at the effective period is taken from the spectrum to give the equivalent elastic SDOF's displacement. By comparing the ratio of the actual nonlinear SDOF's displacement with the equivalent elastic system's, the DRF is computed, as shown in Figure 8. In addition to computing the median DRF from each of the simulations described above, the distribution of DRF vs. ductility can also be considered by performing vertical statistics on the dataset, as outlined in Figure 8. This is particularly useful when characterising the dispersion of the DRF to assist in making probabilistic considerations within displacement-based assessment methods such as Welch *et al.* [2014] and Sullivan *et al.* [2014]. The ground motion records used in this study consist of the artificial set proposed in a similar study by Pennucci *et al.* [2011] and the four sets of ten natural ground motion records outlined in Maley *et al.* [2013].

Since the calibration looks at the variation in SDOF properties, an appropriate range of values must be determined for the calibration. These are as follows.

- A total of 50 effective periods (T_i) are considered between 0.2 and 4 s, as this corresponds to a reasonable range of expected values in EBF structures.
- A total of 50 force reduction factors (R) are considered between 1 and 5, as this is deemed to be an acceptable range for the EBF system.
- A total of 50 ground motions are selected, including a set of 10 artificial records and 40 natural ground motions records covering both EC8 soil types A and C, and displacement spectrum corner periods of 4 and 8 s [Maley *et al.*, 2013].

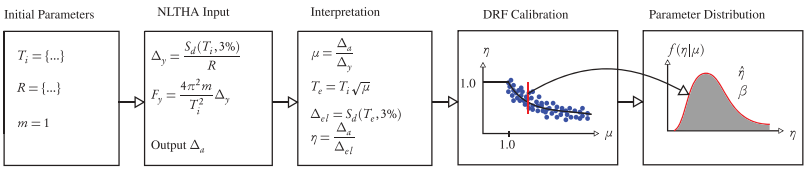

FIGURE 8 DRF calibration methodology.

Note that DRF data was only maintained if the effective period lay prior to the corner period of the displacement spectrum, so as not to be influenced by spectral shape effects identified by Pennucci *et al.* [2011].

Using the above parameters, the SDOF model can be constructed for NLTH analyses with an appropriate ground motion record and the analysis is carried out at a numerical integration time step of 0.002 s. The elastic damping (ξ) considered for the SDOF system was set to 3% and this was applied as tangent stiffness proportional damping following the recommendations of Priestley *et al.* [2007]. Since a typical value for the elastic damping in steel structures is 3% as opposed to 5%, which is more typical of reinforced concrete structures [Chopra, 2012], a value of 3% has been adopted here. In order to construct the 3% damped elastic design spectrum from those specified in design codes, the displacement scaling factor proposed in Eurocode 8 may be used, which is given as follows:

$$R_\xi = \sqrt{\frac{10\%}{5\% + \xi}}, \tag{13}$$

where for a damping of 3%, Equation 13 increases the spectral demands accordingly. Hence, the DRF expression presented here is only applicable for the design of structures where 3% tangent stiffness proportional elastic damping is considered in conjunction with a typical 3% damped elastic spectrum.

3.3.2. Calibration of DRF Expression for EBF Structures. Collecting the data from the suite of NLTH analyses previously highlighted, the complete dataset is compiled and shown in Figure 9a. In order to examine the dataset in detail, the data is binned at ductility increments of 0.1, which allows the computation of the median and dispersion values of DRF vs. ductility. The median value of the data is determined from each of the bins and plotted in Figure 9a, for which the DRF expression to be used in DDBD will be fitted. Also shown in Figure 9a is an example of the distribution of the DRF at a ductility of 2.15. A lognormal distribution is assumed for the data which passes the Lilliefors goodness-of-fit test at the 5% significance level. Figure 9b shows the dispersion associated with each of the data bins versus ductility, where it is seen to plateau at around 0.35 above a ductility of 1.5, where the reduction in dispersion decreases as the ductility approaches unity, since no dispersion is expected for linear elastic systems. The dispersion is reported here as it is expected that

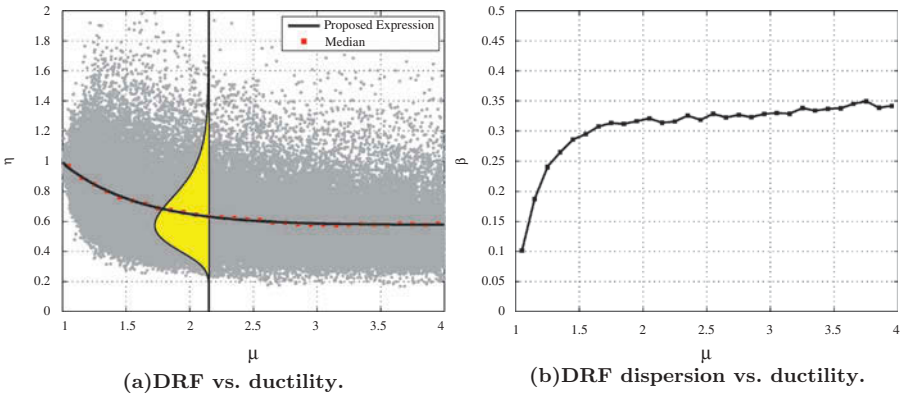

(a)DRF vs. ductility. (b)DRF dispersion vs. ductility.

FIGURE 9 DRF results.

it could be useful for the eventual realisation of probabilistic displacement-based design and assessment methods (see, for example, Welch *et al.*, [2014]). The value of 0.35 is reasonably high but is also in line with values proposed in FEMA P-58 [FEMA P58-1, 2012], suggesting that the results obtained here are in line with those obtained elsewhere.

Using the median values form each of the bins plotted in Figure 9a, an expression can be fitted in order to provide a simple expression to calculate the DRF for EBF structures. This expression, which is also plotted in Figure 9a, is given previously in Equation (8) and corresponds to the DRF expression to be used for EBF structures, assuming 3% tangent stiffness proportional elastic damping and using the modeling recommendations of Section 2.2.1. As is evident from Figure 9a, the proposed expression fits the median of the data very well. Should the user require the corresponding EVD expression for an EBF system, Equation (13) may be be used to calculate the corresponding EVD (ξ) to give:

$$\xi = \begin{cases} 0.03 & \text{for} \quad \mu \leq 1 \\ \frac{0.10}{(2.16\exp(-1.61\mu)+0.56\exp(0.01\mu))^2} - 0.07 & \text{for} \quad \mu > 1 \end{cases}, \tag{14}$$

where μ is given by Equation (3). However, as per the findings of Pennucci *et al.* [2011], Equation (14) is to be used together with the displacement scaling factor given in Equation (13).

3.4. Case Study Design and Assessment of SDOF EBFs using DDBD

Using the DDBD procedure for SDOF structures outlined in Section 3.2 in conjunction with the calibrated DRF expression of Section 3.3, the case study structures of Section 2.1 can be redesigned using DDBD. The geometry, material properties and design seismicity of the case studies is maintained and the resulting designs are shown in Table 3. As outlined in Section 3.2, these structures were sized by first determining their yield drift and drift capacity as per Equations (4) and (7), respectively. The resulting ductility is used to calculate the corresponding DRF in accordance with Equation (8), and the design base shear is determined from Equation (10). The EBF link members are the sized according to Equation (11) and the resulting designs are shown in Table 3. In general, it is observed that the section sizes resulting from DDBD are on average a little larger than those resulting from using Eurocode 8 and ASCE 7-10.

Similar to Section 2.2.4, a pushover analysis on each of the case study structures presented in Table 3 is performed using the numerical model outlined in Section 2.2.1 to evaluate the demand to capacity ratio of the link plastic chord rotation at the design drift level. By setting the design procedure up in terms of displacements, DDBD aims to define the target displacement of the structure in terms of material limit states and expected ductility capacities, which are then used to determine design forces and size the structure in one step, as opposed to the iterative procedures outlined in design codes if the deformation limits are not respected. For each of the designs, the SDOF EBF is subjected to a displacement controlled pushover analysis to the design drift. At this drift, the link plastic chord rotation is noted and compared with the plastic chord rotation capacity of 0.08 rad specified for short link EBFs. Figure 10 shows the ratio between these two, where it is immediately obvious that DDBD provides design solutions that are all within the specified capacity, but also consistently at the same level of demand/capacity ratio, with the ratio always just less than unity. When comparing to the designs outlined in Section 2.1, it is seen how the DDBD method presented here provides a more consistent design solution than existing design code approaches, which had a large variation in demand to capacity ratio for different configurations and tended to initially exceed the design link capacity, especially in the

TABLE 3 Case study designs according to DDBD

Case	e [m]	B [m]	h [m]	f_y [MPa]	m [t]	DDBD		
						Link	Brace	Column
1	0.4	7	3.2	275	150	HE260B	HE200B	HE160B
2	0.6	7	3.2	275	150	HE260B	HE200B	HE160B
3	0.8	7	3.2	275	300	HE240M	HE200M	HE200B
4	1.2	7	3.2	275	300	HE240M	HE200M	HE200B
5	0.4	7	3.2	460	250	HE240B	HE240B	HE160B
6	0.6	7	3.2	460	250	HE240B	HE220B	HE160B
7	0.8	7	3.2	460	500	HE240M	HE220M	HE200B
8	1.2	7	3.2	460	500	HE240M	HE220M	HE200B
9	0.4	5	3.2	460	250	HE200M	HE200B	HE180B
10	0.6	5	3.2	460	250	HE200M	HE200B	HE180B
11	0.8	5	3.2	460	500	HE300M	HE240B	HE240B
12	1.2	5	3.2	460	500	HE260M	HE220B	HE220B
13	0.4	5	4	275	150	HE240M	HE200B	HE200B
14	0.6	5	4	275	150	HE240M	HE200B	HE200B
15	0.6	5	4	275	300	HE360M	HE220B	HE260B
16	1.2	5	4	275	300	HE280M	HE200B	HE220B

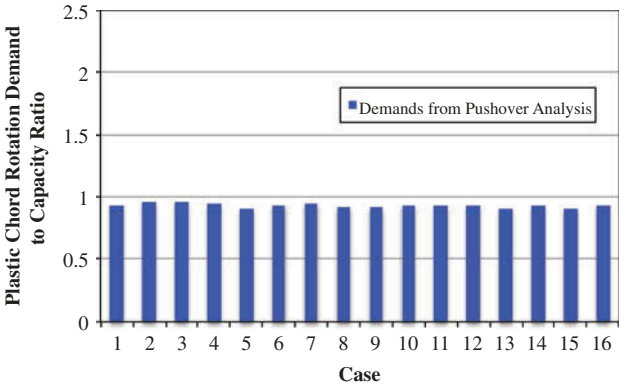

FIGURE 10 Demand to capacity ratio of link plastic chord rotation of DDBD solutions.

case of EC8. In addition, no analysis program was required to design the sections (apart from the pushover analyses to evaluate the design solutions and provide the data shown in Figure 10). In addition, no iteration of designs was required and a complete design can be carried out on one single design spreadsheet. This highlights the added benefits of using DDBD for the seismic design of EBF structures.

3.5. Extension of DDBD to MDOF Structures

The previous section outlined the process of designing a SDOF EBF structure for a specified target displacement and how case study designs showed that this approach led to more consistent design solutions than current design code approaches. This section takes this

method for SDOF systems and extends it to the design of MDOF EBF structures. The following subsections describe the relevant additions to complete the DDBD process or MDOF EBFs with reference to Figure 7. However, for a detailed step-by-step description of the methodology, readers are referred to Sullivan [2013a,]

3.5.1. Design-Displaced Shape Profile. In addition to the yield drift and drift capacity of an individual story, a target displaced shape is required for MDOF EBF structures, with the displaced shape scaled to the limit-state drift capacity of the most critical floor in the building. Sullivan [2013a] proposed the following expression for the limit-state profile, which gives a linear displaced shape at elastic displacement levels and a more parabolic shape for higher intensity levels:

$$\Delta_{ls,i} = \begin{cases} min\,(\theta_c)\,H_i & \text{for} \quad min(\theta_c) \leq min(\theta_y) \\ min\,(\theta_c)\,H_i + \left(min\,(\theta_c) - min\left(\theta_y\right)\right) H_i \frac{2H_n - H_i}{2H_n - H_1} & \text{for} \quad min(\theta_c) > min(\theta_y) \end{cases}, \tag{15}$$

where the terms $min(\theta_y)$ and $min(\theta_c)$ refer to the minimum value of both yield and capacity drift calculated over the entire height of the structure. This expression was shown by Sullivan [2013a] to match the displacement profiles obtained at various intensities for a 6-story EBF structure tested by Whittaker *et al.* [1987] and because the design displacement profile becomes more non-linear at increasing levels of ductility demand, it is considered more accurate than the invariant displacement profiles predicted from elastic modal analyses (currently used in code design methods).

3.5.2. Higher Mode Effects. In addition to the definition of the displaced shape of the EBF for an assumed first mode structural response, consideration must also be given to the possibility of higher modes of vibration increasing story drift demands. In order to account for this higher mode response, two steps are taken in the DDBD procedure to ensure excessive drifts do not develop in the upper floors.

1. The target limit-state displaced shape is scaled down to account for increased drifts associated with higher mode response (see Figure 11), so that as the drift contribution of the higher modes increases, the first mode displaced shape is scaled down

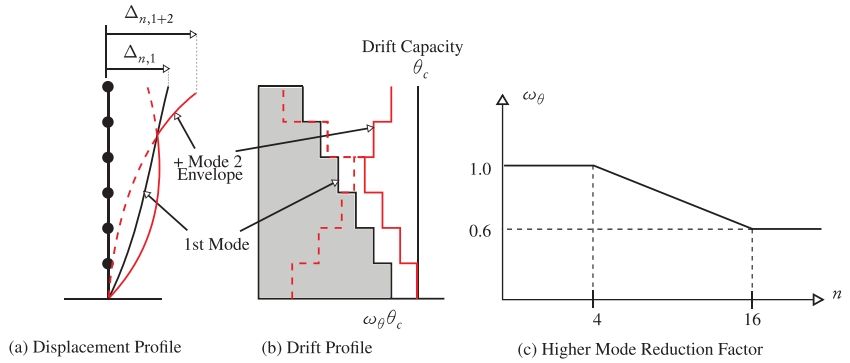

FIGURE 11 Accounting for higher mode influence on EBF interstory drift profiles (adapted from Sullivan *et al.*, 2012).

by such an amount that results in the combined drift of all modes remaining within the target drift limits.

2. A fraction (typically 10%) of the design base shear is lumped at the roof level when setting the required design strength distribution to increase strength in upper floors and achieve relatively uniform drift demands over the structure height.

This scaling referred to in point 1 above is done by the application of the scaling factor ω_θ, in line with recommendations of Sullivan *et al.* [2012], which is illustrated in Figure 11 for EBFs, to the limit state displaced shape $\Delta_{ls,i}$ to give the design displaced shape as:

$$\Delta_i = \omega_\theta \Delta_{ls,i}. \tag{16}$$

As shown in Figure 11, this higher mode scaling factor is a function of the number of stories (n) in the structure. For the adjustment of the lateral force vector to ensure more uniform displacement response (point 2 above), this will be discussed in tandem with the discussion of the lateral force application in Section 3.5.4.

3.5.3. DDBD of EBFs Using Proposed DRF. Section 3.3 proposed a new DRF expression for EBF structures. In order to implement Equation (8) into DDBD, some additional considerations are required when designing MDOF EBF structures. Equation (8) relates the μ of the EBF to the η and for the case of a SDOF EBF, the ductility varies along the height of the structure. Sullivan [2013a] proposed to find the equivalent SDOF system's ductility (μ) and implement this to find the equivalent SDOF system's DRF (η). However, since the design displaced shape of the EBF is proposed to be of a parabolic shape, the upper stories of high rise EBF's tend to remain elastic for the design displacement. This is observed in the design case study structures summarised in Tables 5 and 6. If the equivalent SDOF system's μ is calculated through the weighting of work done at each level of MDOF structure and then used in Equation (8), for which an equivalent SDOF μ greater than unity is computed, this inherently assumes that the expression given in Equation (8) for μ greater than 1 is valid over all ductility values, which according to Equation (8) is not the case. It is therefore proposed to calculate the η_i values associated with target μ_i at each floor of the MDOF EBF structure and then compute a weighted equivalent SDOF η value according to the work done at each level. This means that for values of μ_i less than one, Equation (8) is being implemented correctly and this is reflected in the equivalent SDOF η value. The equivalent SDOF η is therefore calculated as follows:

$$\eta = \frac{\sum_{i=1}^{n} V_i \theta_i \eta_i}{\sum_{i=1}^{n} V_i \theta_i}, \tag{17}$$

where V_i and θ_i are the design story shear and design interstory drift at a given story i, respectively.

3.5.4. Design Base Shear and Lateral Force Distribution. The design base shear obtained from Equation (10) is then distributed along the height of the structure in accordance with:

$$F_i = \begin{cases} k \frac{m_i \Delta_i}{\sum_{i=1}^{n} m_i \Delta_i} V_b & \text{for} \quad i < n \\ (1-k)V_b + k \frac{m_i \Delta_i}{\sum_{i=1}^{n} m_i \Delta_i} V_b & \text{for} \quad i = n \end{cases}, \tag{18}$$

where k is a term that is taken as 0.9 for structures with 6 or more stories to account for higher mode effects, as previously discussed in Section 3.5.2. This essentially takes 10%

of the design base shear and places it at roof level to increase the design shear forces in the upper stories and mitigate excessive drift amplification due to higher mode effects. The individual story shears are then determined by summing all the lateral forces for each of the upper stories as follows:

$$V_i = \sum_{j=i}^{n} F_j. \tag{19}$$

3.6. Summary

To summarize the design procedure outlined in the previous sections, Figure 12 presents a flowchart of the steps involved in the DDBD of EBF structures with reference to each of the expressions proposed in the previous sections and providing further details about the DDBD process. A step-by-step example for the DDBD of EBFs has been provided in Sullivan [2013a] for a five-story EBF building, and the reader is reminded that the proposals here supersede those of Sullivan [2013a], but the general approach remains the same nonetheless, where the proposed modifications here give more confidence in the numerical modeling and determination of an appropriate DRF via an experimentally calibrated hysteresis model. The equations described above and in more detail in Sullivan [2013a] can be easily implemented in a spreadsheet and thus the procedure is considered relatively simple. Nevertheless, it is also recognised that the DDBD procedure for EBFs does include considerably more steps than force-based alternatives such as the equivalent lateral force method. As such, future research could aim to simplify the procedure, possibly in line with the proposals made by Sullivan [2013b] for the DDBD of RC frame buildings.

4. Design of Case Study Buildings

In order to investigate the performance of the DDBD guidelines, a series of case study structures are designed using the proposed method. These structures vary in height from 1–15 stories, and are also designed separately for two spectral shapes. The designs are then evaluated using NLTH analysis of the various structures to demonstrate the effectiveness of the method.

4.1. Description of Case Study Structure

4.1.1. Structure Layout. The case study structures examined in this study are shown in Figure 13, which consists of uniform bay widths of 7 m in each direction and a uniform story height of 3.5 m. The variations of this structural configuration are structures with 1, 5, 10, and 15 stories. In each case, the structure is assumed to have 4 EBFs as part of the lateral load resisting system in each direction. The seismic weights considered for the structure are noted in Figure 13 with each story having a weight of 6,240 kN, while the weight of the roof is taken as 5,500 kN. European steel section sizes are used throughout and the grade of steel is chosen to be Grade 450 steel with nominal strength 450 MPa, where the expected value of the material is taken as 528 MPa in line with Badalassi *et al.* [2011], as DDBD requires actual material strength values to be used in place of nominal values. Sullivan *et al.* [2012] recommends that 1.1 times the nominal yield strength of steel may be used as the expected strength in the absence of more detailed material property information or material coupon test results.

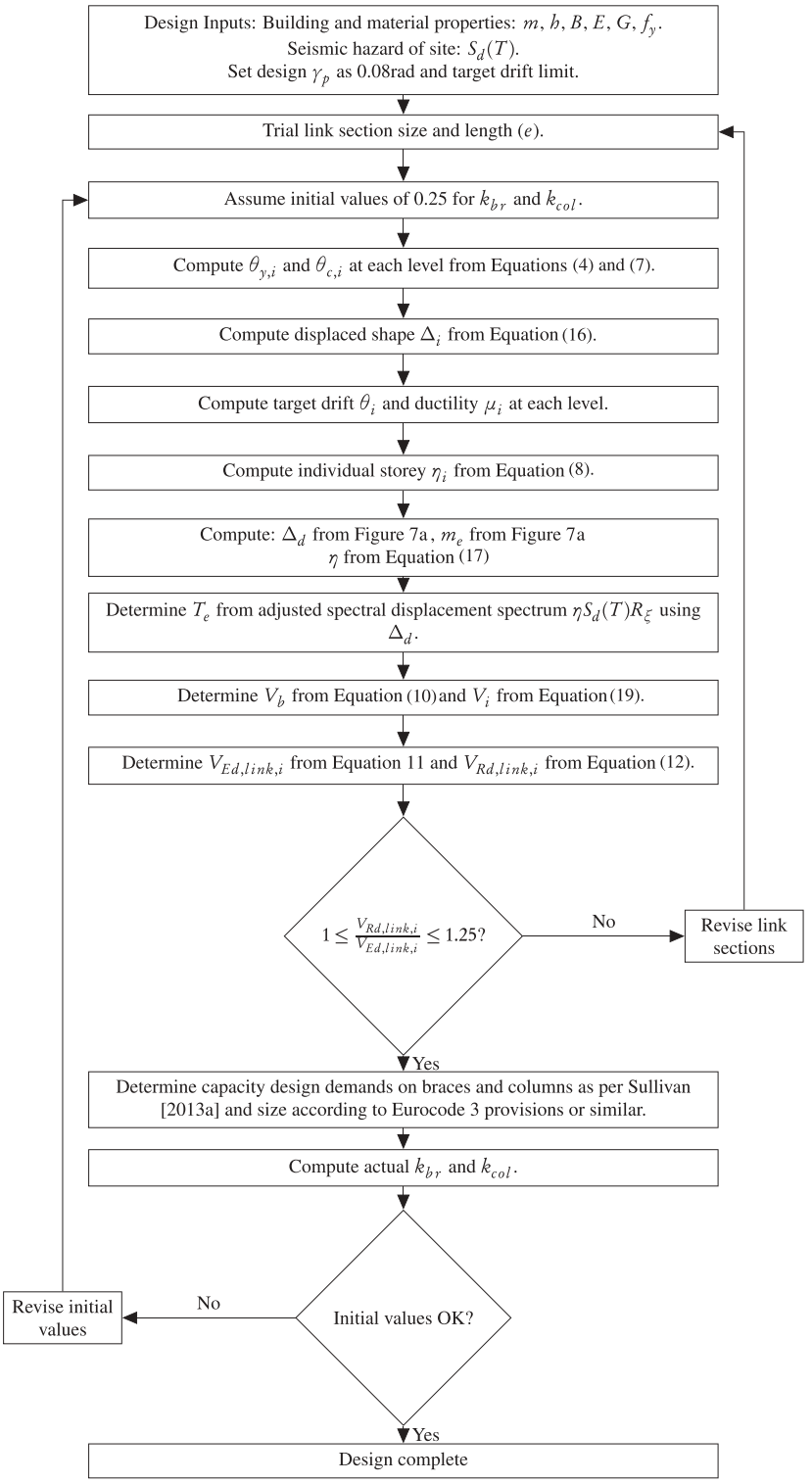

FIGURE 12 Flowchart for the DDBD of EBF structures.

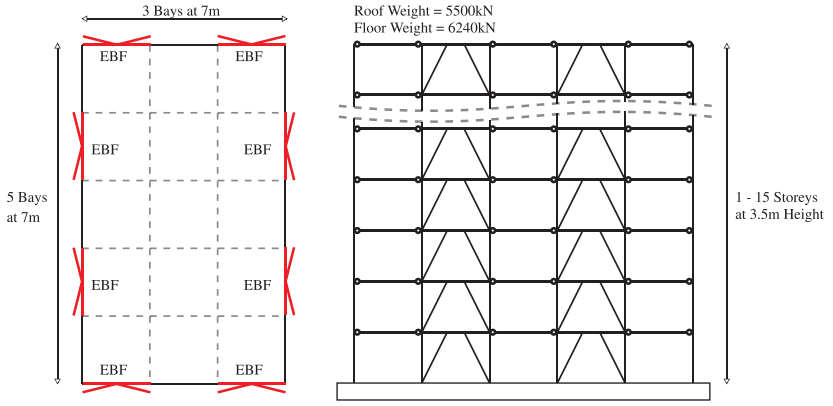

FIGURE 13 Plan and elevation layout of case study structure.

4.1.2. Seismic Hazard. The seismic hazard considered for the design of the case study structures consists of two different design spectra taken from Maley *et al.* [2013] and are shown in Figure 14. These spectra are EC8 type 1 spectra with soil type A and C, as per the soil type definitions outlined in EC8, modified such that both spectra have a spectral displacement corner period (T_d) of 8 s. The reason for this long corner period, as opposed to 2 s recommended by EC8, is that Faccioli *et al.* [2004] demonstrated that longer corner periods can be expected in certain regions of Italy (and elsewhere), and therefore the study by Maley *et al.* [2013] considered the effects of this in determining suitable design spectra. Both spectra have an equivalent peak ground acceleration (PGA) of 0.4 g on hard rock, which means soil type A spectrum has a PGA of 0.4 g whereas the soil type C has a slightly larger PGA due to soil effect amplification factors. These spectra shown in Figure 14 correspond to those used in the study by Maley *et al.* [2013] for which sets of ground motions were selected, scaled, and are presented and discussed in Section 5.2.

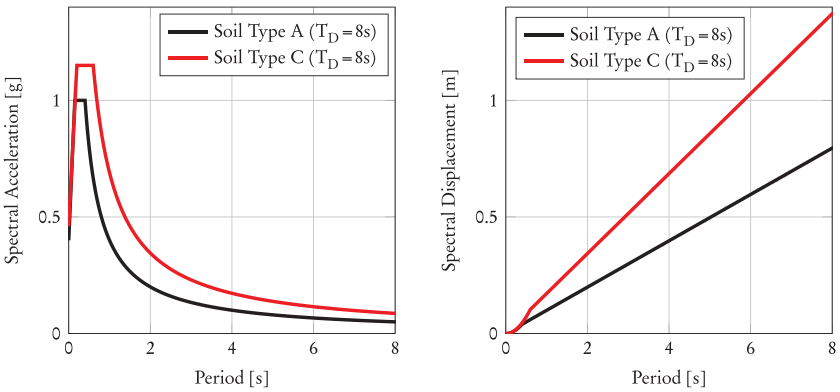

(a) Design acceleration spectra. (b) Design displacement spectra.

FIGURE 14 Design seismic hazard.

4.2. Design Criteria

The design criteria set out in this study are in accordance with the model code DBD12 [Sullivan *et al.*, 2012], where the interstory drift limits of 2.5% are implemented to protect nonstructural elements in addition to the plastic chord rotation limits of the links are set at 0.08 rad, although as will be seen in Section 4.3, the plastic chord rotation limits govern in each design scenario. For brevity, only peak interstory drift and peak displacement are reported for each EBF design, along with the performance of the capacity design of the brace and column elements.

4.3. Case Study Designs

Each of the structure types considered were designed to both design spectra shown in Figure 14. Table 4 summarizes the DDBD parameters used for the design of each structure in accordance with the procedure summarised in Figure 12, in addition to the total mass of structural steel required (M), as well as the final resulting base shear coefficient (C_s). For both of these parameters M and C_s reported in Table 4, it can be seen that the soil type C design requires more steel than that of soil type A, which is to be expected as the spectral ordinates were higher than soil type A in Figure 14. Similarly, the base shear coefficients C_s are much higher for the case of the soil type C design and tend to decrease with increasing number of stories.

TABLE 4 DDBD parameters

Design Parameter		1 Story	5 Story	10 Story	15 Story
		Soil Type A			
Δ_d	[m]	0.031	0.061	0.156	0.336
m_e	[T]	140.2	419.4	1341.3	1981.7
H_e	[m]	3.5	7.7	23.1	34.3
μ	[–]	3.40	2.36	1.71	1.26
η	[–]	0.588	0.662	0.812	0.858
T_e	[s]	0.48	0.84	1.72	3.52
M	[T]	108.2	426.1	3445.0	5295.0
V_b	[kN]	748.7	1440.0	2788.4	2309.1
C_s	[%]	54.4	32.0	18.1	9.9
		Soil Type C			
Δ_d	[m]	0.042	0.094	0.296	0.390
m_e	[T]	140.2	422.6	1340.1	1987.2
H_e	[m]	3.5	7.7	23.1	34.3
μ	[–]	3.07	2.93	1.93	1.34
η	[–]	0.593	0.644	0.765	0.847
T_e	[s]	0.46	0.76	2.02	2.40
M	[T]	123.4	624.1	3885.4	8864.8
V_b	[kN]	1085.9	2706.0	3837.6	5316.4
C_s	[%]	79.0	60.2	24.9	22.9

From these structures designed using DDBD in Table 4, the resulting cross section member sizes for each design along with link length (e), design drift (θ_d), drift capacity (θ_c), story design ductility demand (μ), and overstrength (Ω_{link}) of the provided to the required link strength are reported in Tables 5 and 6 for both soil types A and C, respectively. It can be observed that as the number of stories increases, the design ductility of the upper stories reduces and the upper stories are expected to respond elastically during seismic loading and hence, concentrate the inelastic behavior in the lower stories of the structure. This is a consequence of using the target displaced shape proposed in Equation (15), as the parabolic nature of the displaced shape means that the upper stories are expected to be subjected to relatively little relative displacement and hence, interstory drift in the first mode. In order to increase the target ductility in the upper stories, the displaced shape could be adjusted to give a more linear shape. By doing this, however, the contribution of higher modes of vibration may become more prominent and end up amplifying the interstory drift in the upper and bottom stories beyond the target design drift.

5. Verification Analysis of Case Study Buildings

In order to evaluate the DDBD method for EBF structures outlined in Section 3, the eight different structure typologies summarized in Tables 5 and 6 are evaluated through nonlinear time-history (NLTH) analyses using a series of spectrum compatible ground motion records for both design spectra. This section first discusses the additional numerical modeling parameters required for the dynamic analyses of the EBF structures, followed by the ground motion sets to be used for the NLTH analyses. The results of the NLTH analyses are then presented for each case to evaluate the DDBD methods robustness in the design of EBF structures.

5.1. Dynamic Analysis Modeling Parameters

A 2D model consisting of force-based fiber elements is developed in OpenSees [McKenna *et al.*, 2000] for the design verification using the EBF link numerical modeling procedure outlined in Section 2.2.1. For the beam and column elements, force-based fiber elements with 7 integration points per element are used for these members with the Giuffre Menegotto-Pinto material model. A total of 20 fibers are used along both the web depth and flange width of sections, while 5 fibers are used along the thickness. Second-order geometry effects (P-Delta) are modeled through the use of a dummy column outside of the structure which is pinned at each floor level to model the gravity loading of the structure not attributed directly to the EBF frame being modeled. Since the case study structure is symmetric in both directions, significant torsional response is not anticipated and only one EBF is modeled with one quarter of the tributary mass and loads are assigned to this frame. The masses are therefore lumped at each floor at each of the exterior column nodes, which are also pinned at the base connection. A Newmark integration scheme was adopted with a time step of 0.001 s. For the elastic damping model, 3% Rayleigh tangent stiffness proportional damping is assigned to the first and third modes of vibration of the structures. The lateral resistance of the internal gravity system is assumed to be negligible and is not modeled.

5.2. Ground Motion Sets

As mentioned previously in Section 4.1.2, the design spectra used in this study consist of those used in a similar study by Maley *et al.* [2013]. In that study, a series of ground motion

TABLE 5 Soil Type A Design

Level	Link	Brace	Column	e [m]	θ_d [%]	θ_c [%]	μ	Ω_{link}
			1 Story					
1	HE200A	HE180B	HE160B	0.550	0.89	0.89	3.40	1.207
			5 Story					
5	HE200A	HE160B	HE140B	0.500	0.39	1.15	0.68	1.191
4	HE180B	HE200B	HE180B	0.600	0.57	1.28	0.96	1.037
3	HE220B	HE200B	HE180M	0.800	0.75	1.50	1.28	1.075
2	HE240B	HE220B	HE220M	0.800	0.93	1.37	2.05	1.083
1	HE260B	HE240B	HE240M	0.800	1.11	1.22	3.57	1.138
			10 Story					
10	HE450B	HE200B	HE180B	0.600	0.23	2.03	0.17	1.071
9	HE500B	HE200B	HE200B	0.600	0.31	1.98	0.24	1.063
8	HE500B	HE220B	HE240B	0.800	0.39	2.16	0.31	1.023
7	HE500B	HE240B	HE280B	0.800	0.46	2.04	0.41	1.092
6	HE450B	HE220M	HE340B	0.800	0.54	1.88	0.56	1.095
5	HE400B	HE220M	HD360 × 196	0.800	0.62	1.77	0.72	1.072
4	HE360B	HE220M	HD400 × 237	0.800	0.70	1.65	0.95	1.071
3	HE360B	HE240M	HD400 × 262	0.800	0.77	1.46	1.41	1.103
2	HE360B	HE240M	HD400 × 314	0.800	0.85	1.31	2.16	1.107
1	HE360B	HE240M	HD400 × 382	0.800	0.93	1.16	3.81	1.131
			15 Story					
15	HE360B	HE200B	HE160B	1.500	0.36	3.84	0.17	1.081
14	HE400B	HE220B	HE180B	1.500	0.43	3.76	0.21	1.071
13	HE450B	HE220B	HE200B	1.500	0.50	3.65	0.26	1.162
12	HE450B	HE220B	HE360B	1.500	0.57	3.60	0.30	1.103
11	HE450B	HE220B	HE300B	1.500	0.64	3.51	0.35	1.104
10	HE450B	HE240B	HE320B	1.500	0.71	3.37	0.43	1.159
9	HE400B	HE240B	HE400B	1.500	0.78	3.27	0.50	1.042
8	HE400B	HE260B	HD400 × 237	1.500	0.85	3.16	0.59	1.115
7	HE360B	HE280B	HD400 × 262	1.500	0.92	3.05	0.69	1.011
6	HE340B	HE220M	HD400 × 287	1.400	0.98	2.77	0.85	1.059
5	HE320B	HE220M	HD400 × 347	1.400	1.05	2.66	0.99	1.067
4	HE320B	HE220M	HD400 × 382	1.400	1.12	2.53	1.21	1.057
3	HE320B	HE220M	HD400 × 421	1.400	1.19	2.40	1.50	1.051
2	HE320B	HE220M	HD400 × 463	1.400	1.26	2.26	1.92	1.056
1	HE320B	HE220M	HD400 × 463	1.400	1.33	2.11	2.63	1.072

sets were selected in order to conduct NLTH verification analysis and are used here and the individual spectra for each set along with their respective means are shown in Figure 15 for both spectral acceleration and spectral displacement.

TABLE 6 Soil Type C Design

Level	Link	Brace	Column	e [m]	θ_d [%]	θ_c [%]	μ	Ω_{link}
			1 Story					
1	HE180B	HE200B	HE160B	0.700	1.19	1.19	3.07	1.031
			5 Story					
5	HE260B	HE220B	HE160B	0.800	0.48	1.69	0.62	1.082
4	HE300B	HE240B	HE220B	1.000	0.73	1.90	0.96	1.052
3	HE340B	HE300B	HE240M	1.000	0.97	1.78	1.54	1.013
2	HE400B	HE300B	HE260M	1.000	1.22	1.66	2.37	1.167
1	HE400B	HE300B	HE300M	1.000	1.46	1.51	3.95	1.128
			10 Story					
10	HE400B	HE200B	HE160B	1.200	0.45	3.01	0.28	1.063
9	HE450B	HE220B	HE220B	1.200	0.60	2.93	0.38	1.078
8	HE450B	HE240B	HE280B	1.400	0.74	3.12	0.49	1.011
7	HE450B	HE260B	HE340B	1.500	0.89	3.16	0.62	1.028
6	HE450B	HE220M	HE450B	1.500	1.03	3.00	0.80	1.138
5	HE400B	HE240M	HD400 × 237	1.500	1.18	2.85	1.03	1.081
4	HE400B	HE240M	HD400 × 287	1.500	1.32	2.70	1.34	1.019
3	HE450B	HE240M	HD400 × 347	1.500	1.46	2.52	1.81	1.152
2	HE450B	HE240M	HD400 × 421	1.500	1.61	2.36	2.48	1.138
1	HE450B	HE260M	HD400 × 509	1.500	1.75	2.19	3.68	1.150
			15 Story					
15	HE500M	HE180M	HE200B	1.700	0.38	4.53	0.15	1.022
14	HE600M	HE200M	HE240B	1.700	0.47	4.42	0.19	1.025
13	HE650M	HE200M	HE260B	1.700	0.55	4.30	0.24	1.037
12	HE650M	HE220M	HE340B	1.700	0.64	4.16	0.29	1.028
11	HE650M	HE220M	HD400 × 262	1.700	0.72	4.08	0.34	1.024
10	HE650M	HE240M	HD400 × 287	1.700	0.81	3.93	0.41	1.074
9	HE600M	HE240M	HD400 × 314	1.700	0.89	3.81	0.48	1.050
8	HE550M	HE240M	HD400 × 347	1.700	0.98	3.67	0.57	1.044
7	HE500M	HE240M	HD400 × 421	1.700	1.06	3.54	0.67	1.043
6	HE600B	HE240M	HD400 × 509	1.700	1.15	3.33	0.83	1.026
5	HE550B	HE260M	HD400 × 551	1.700	1.23	3.17	1.01	1.047
4	HE550B	HE260M	HD400 × 634	1.700	1.32	2.99	1.25	1.033
3	HE550B	HE260M	HD400 × 744	1.700	1.40	2.82	1.59	1.027
2	HE550B	HE260M	HD400 × 818	1.700	1.49	2.65	2.09	1.032
1	HE550B	HE260M	HD400 × 900	1.700	1.57	2.48	2.92	1.047

5.3. Analysis Results

The following sections plot the peak interstory drift and peak displacement for each of the case study structures designed to the different design spectra. The design drift and displaced shape are plotted with the individual ground motion responses and mean of these

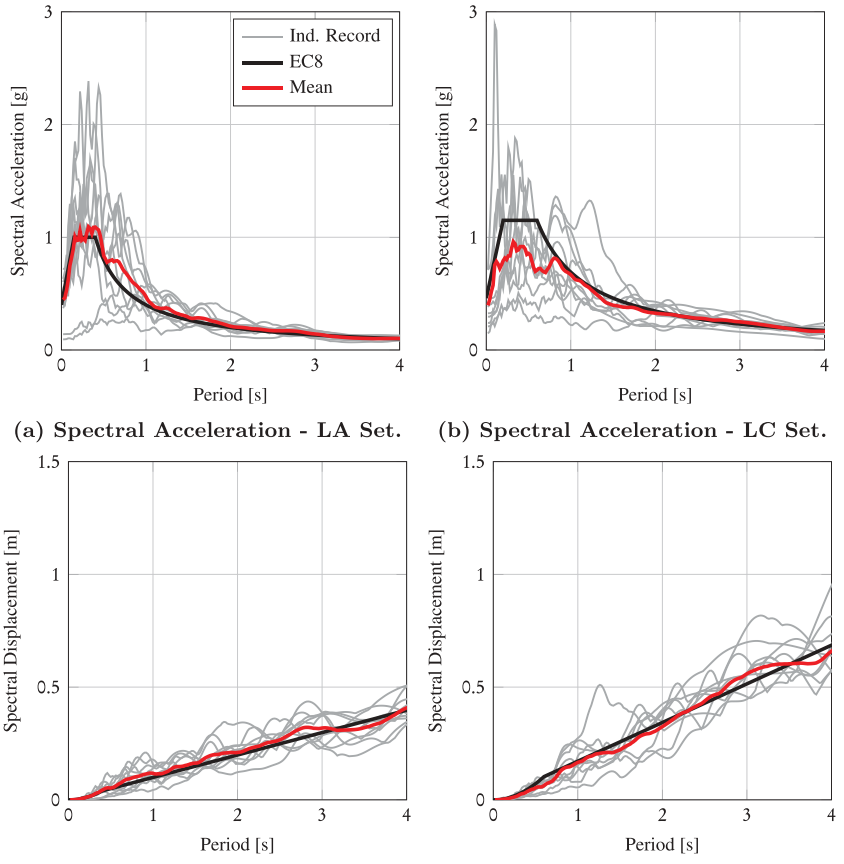

(a) Spectral Acceleration - LA Set. (b) Spectral Acceleration - LC Set.

(c) Spectral Displacement - LA Set. (d) Spectral Displacement - LC Set.

FIGURE 15 Design spectra of compatible ground motions from Maley *et al.* [2013].

ground motions to evaluate the performance of the DDBD method for each of the designs considered.

5.3.1. Interstory Drift. Figure 16 shows the interstory drift profiles for the case study structures. It can be seen that the DDBD method has worked very well in controlling the interstory drift of the EBF structures for each of the case study buildings. Note that for the single story EBFs in Figures 16a and 16e, the link capacity drift (θ_c) and design drift (θ_d) correspond to the same story drift as per Table 5 and 6 and hence, only the line for θ_c is visible in the plots. However, the response to soil type A ground motions appears to be a lot closer to the link capacity than that of the soil type C responses. Part of the reason could be greater higher mode effects that result for this spectral shape (see Roldan *et al.*, 2014; Nievas and Sullivan, 2015). In general, the results obtained are encouraging. The design drift profile set out in DDBD has ensured that the interstory drift does not exceed the link capacity in all cases. In addition to this, the design profile has limited the interstory drift contributions of the higher modes of vibration. For example, the interstory drifts observed in the 15-story building in Figure 16h show a slight increase in the drift of the upper floors due to the second mode of vibration's contribution. However, the design displacement profile has been set out in such a way in Section 3.5.1 that this increase in

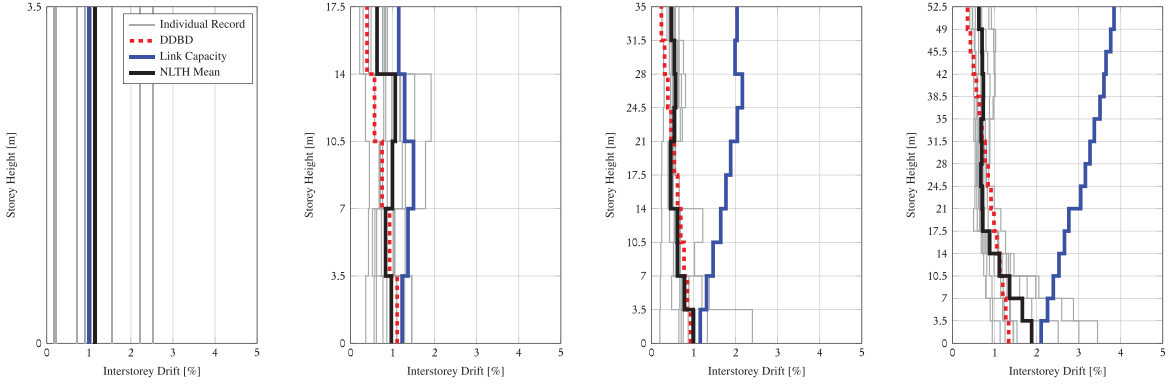

(a) 1 Storey - Soil Type A. (b) 5 Storey - Soil Type A. (c) 10 Storey - Soil Type A. (d) 15 Storey - Soil Type A.

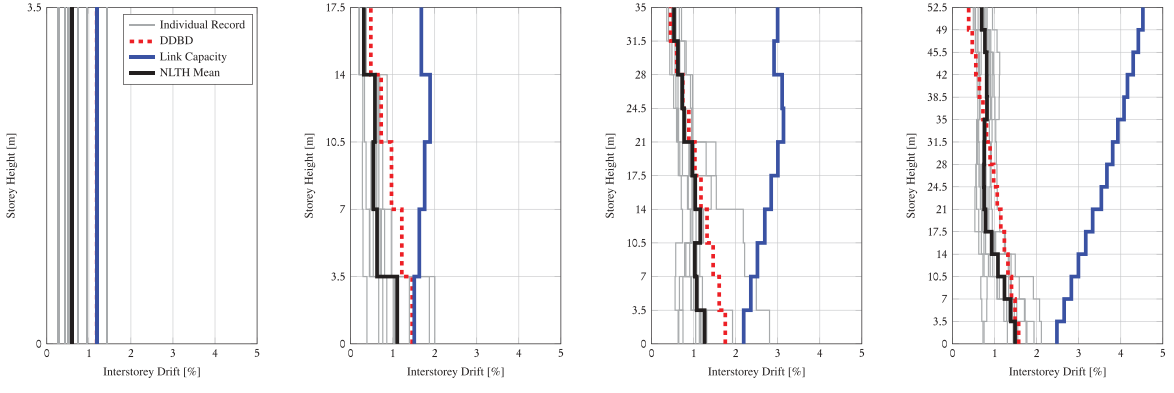

(e) 1 Storey - Soil Type C. (f) 5 Storey - Soil Type C. (g) 10 Storey - Soil Type C. (h) 15 Storey - Soil Type C.

FIGURE 16 Interstory drift response for both ground motion sets.

interstory drift in the upper floors appears to be adequately controlled. The exceedance of the design interstory drift profile in lower floors of Figure 16d is also deemed acceptable as despite this exceedance, the proposed displaced shape was reduced to allow for higher mode drift amplification to be considered such that the modal combination does not exceed the link capacity at any level, as illustrated in Figure 11. Comparing with Sullivan [2013a], drift concentrations for the case of the 15-story structure are not observed here due to the careful control of link overstrength ratio (Ω_{link}) and the overstrength gradient between levels. A limit of 1.25 was proposed here, where looking at the values Tables 5 and 6, this limit is well respected and is reflected in the results shown in Figure 16.

5.3.2. Displacement. Figure 17 shows the maximum displacement response of each of the case study structures examined. As can be seen for each of the cases, the displaced shape of the EBF's remains quite close to that of the target design displacement except over the upper stories of the structure which adopt a relatively linear profile. This is attributed to the higher mode reduction factors applied to the displaced shape to prevent excessive drift amplification and also the elastic behavior anticipated in the upper stories, as seen in Tables 5 and 6. Ideally, the section sizes in the upper stories of the taller structures may be sized an a way that would encourage more ductile behavior, as from Figure 16 there is still a lot of drift capacity available before link capacities would begin to be exceeded. One possibility could be to revise the lateral load distribution from that proposed in Equation (18) to an approach similar to that proposed by Roldan *et al.* [2014] for MRF structures showing quite positive results. This approach allows more flexibility in the design story shear distribution while at the same time providing the required base overturning moment as required by the DDBD procedure, although this is a refinement beyond the scope of this article.

5.3.3. Beam and Column Capacity Design. In terms of the capacity design of the brace and column elements outlined in Section 3.2.5, a comparison between the observed and provided axial force capacities is provided in Figure 18, which plots the ratio of the observed mean axial force from NLTH analyses as a ratio to the member capacities. These are plotted vs. the normalized height of each of the case study structures, where the terms in the legend, such as 5-A, indicates the 5-story structure designed for soil type A. Figure 18 shows that the demand to capacity ratios are less than unity in all cases for both braces and columns, demonstrating the effectiveness of the capacity design provisions outlined in Section 3.2.5. Another observation is the slight decrease in the demand to capacity ratio, especially in the case of the 15-story structure designed using the soil type A spectrum. This can be explained by the capacity design assumption that a full mechanism would form over the height of the EBF, which is a worst case scenario that is not very likely. This is recognised in some codes (e.g., AISC 341-10, 2010; CSA S16-09, 2009; NZS 3404, 2007), where a reduction in the amplification of column axial loads is permitted for high rise structures to take this into account. However, since there is no obvious and clear trend in Figure 18 that would suggest a relaxation of capacity design amplification factors for columns in tall EBF structures, no reduction in amplification is suggested here. However, further studies could be conducted to provide more insight on this subject, not only for EBFs but for frame structures in general.

6. Summary and Conclusions

This article developed and verified tools for the DDBD of eccentrically braced steel-frame structures. A review into current design code approaches to the design of a series of SDOF EBFs was carried out to illustrate an important clarification required in Eurocode 8 for

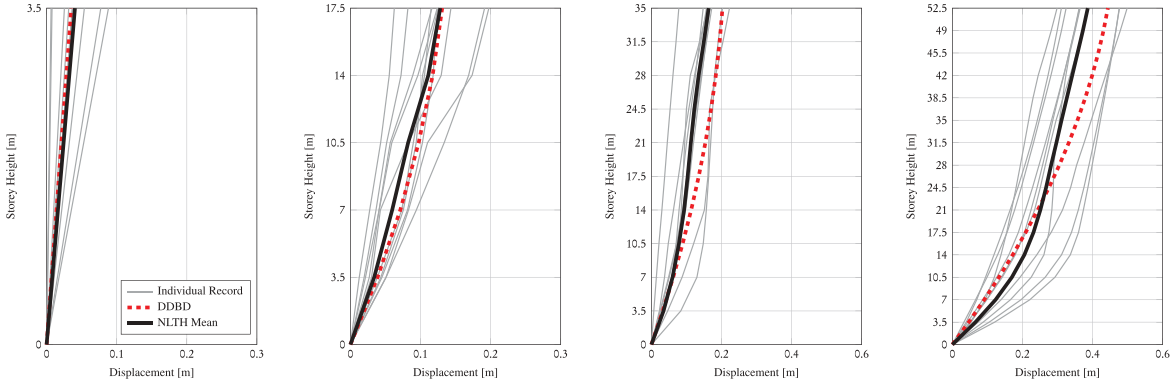

(a) 1 Storey - Soil Type A. (b) 5 Storey - Soil Type A. (c) 10 Storey - Soil Type A. (d) 15 Storey - Soil Type A.

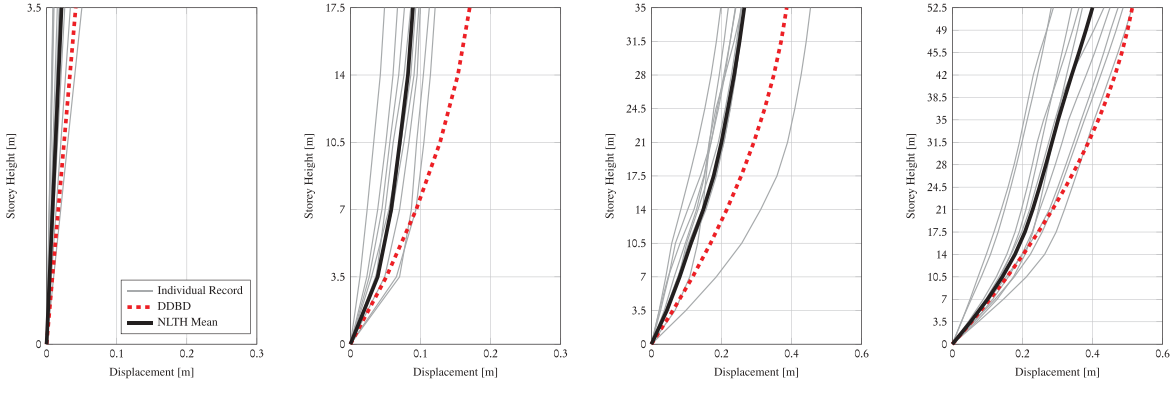

(e) 1 Storey - Soil Type C. (f) 5 Storey - Soil Type C. (g) 10 Storey - Soil Type C. (h) 15 Storey - Soil Type C.

FIGURE 17 Displacement response for both ground motion sets.

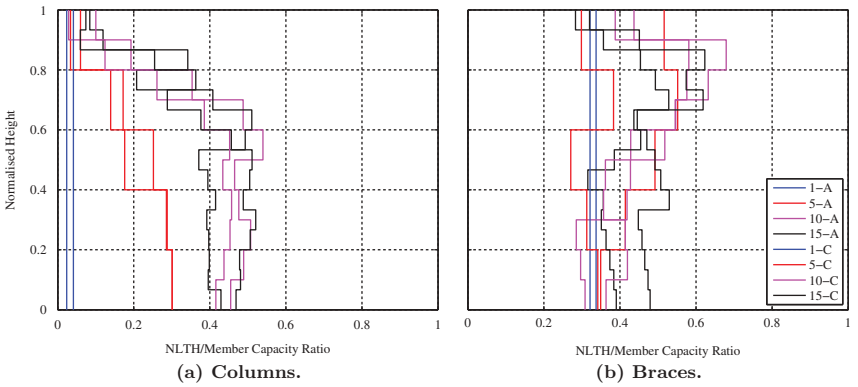

(a) Columns. (b) Braces.

FIGURE 18 Ratio of NLTH axial force to axial force capacity for each design case.

the determination of plastic link demands when using elastic analysis for design. In addition, these design case studies showed that current force-based methods do not provide a direct method to control design deformation demands which then provided motivation for a displacement-based design approach for EBFs. The design method was discussed to present and justify the various steps used in the design procedure. Among these, important refinements include the calibration of a spectral displacement reduction factor to relate the displacement of the inelastic system to that of the equivalent linear system used in DDBD. This was developed using the experimentally calibrated link element model that more accurately represents the behavior of EBF links compared to more simplified bilinear hysteresis models that do not account for isotropic hardening in the links. The complete method was then summarized into a step-by-step flow chart in Figure 12, and a series of case study structures were designed. These included four structure types ranging from a single-story to a 15-story structure, designed for two different spectral shapes. Nonlinear time-history analyses were then used to evaluate each of these design case study structures and the results of the analysis were compared in terms of the control of interstory drift, displaced shape and also the capacity design of the brace and column members. From this study on the design of EBF structures, the following conclusions are made.

- There appear to be shortcomings with the current Eurocode 8 method in terms of accurately controlling link member deformation demands. In addition, it has been demonstrated that unique force reduction (behavior) and displacement amplification factors are not applicable to all types of EBF configurations as the system ductility capacity varies as a function of geometrical and material properties.
- Some discrepancy exists in the computation of design plastic link demands using Eurocode 8 with inadequate account for the localised concentration of deformation demands in the link elements when EBF move into the inelastic range of response. Results obtained using a newly proposed adjustment factor compared well with pushover results and thus the adjustment is recommended for incorporation into Eurocode 8, noting that the US provisions already consider this issue in design.
- A numerical model that captures the behavior of short link elements was proposed, and the results of experimental tests were used to validate the parameters and thus propose relatively simple numerical modeling guidelines for EBF systems that represent the isotropic hardening and hysteretic behavior quite well.

- A spectral displacement reduction factor expression has been developed for EBFs using a newly calibrated hysteretic model for the link members. Information on the dispersion associated with the DRF expression was also provided.
- For each of the case study structures designed, nonlinear time-history analyses using a set of spectrum compatible ground motions and an experimentally validated numerical modeling approach demonstrated the satisfactory performance of each of the case study structures, thus demonstrating the robustness of the DDBD method for the seismic design of EBF structures.
- Existing amplification factors for the estimation of capacity design actions on columns and braces in EBFs have been found to provide adequate protection of these non-dissipative zones during seismic response.

References

AISC 341-05. [2005] Seismic Provisions for Structural Steel Buildings. U.S. Standard, American Institute of Steel Construction, Chicago, Illinois.

AISC 341-10. [2010] Seismic Provisions for Structural Steel Buildings. U.S. Standard, American Institute of Steel Construction, Chicago, Illinois.

AISC 360-10. [2010] Specification for Structural Steel Buildings. U.S. Standard, American Institute of Steel Construction, Chicago, Illinois.

Arce, G. [2002] Impact of higher strength steels on local buckling and overstrength of links in eccentrically braced frames. MSc thesis, The University of Texas at Austin.

ASCE 7-10. [2010] Minimum Design Loads for Buildings and Other Structures. U.S. Standard, American Society of Civil Engineers, Reston, Virginia.

Badalassi, M., Braconi, A., Caprili, S., and Salvatore, W. [2011] Seismic structural performance of EBF - influence of steel yielding stress limitations on collapse modes. *EUROSTEEL 2011*.

Bruneau, M., Anagnostopoulou, M. MacRae, G. A., Clifton, C., and Fussell, A. [2010] "Preliminary report on steel building damage from the Darfield earthquake of September 4, 2010," *Bulletin of the New Zealand Society for Earthquake Engineering* **43**(4), 351–359.

Bruneau, M., Clifton, C., MacRae, G. A., Leon, R., and Fussell, A. [2011] "Steel Building Damage from the Christchurch Earthquake of February 22, 2011," *Bulletin of the New Zealand Society for Earthquake Engineering* Draft, 2011.

Chopra, A.K. *Dynamics of Structures: Theory and Applications to Earthquake Engineering*. Prentice Hall, Englewood Cliffs, New Jersey, 4th edition, 2012.

Clifton, C., Bruneau, M., MacRae, G. A., Leon, R., and Fussell, A. [2011] "Steel structures damage from the Christchurch Earthquake series of 2010 and 2011," *Bulletin of the New Zealand Society for Earthquake Engineering* **44**(4), 297–318.

CSA S16-09. [2009] Design of Steel Structures. Canadian standard, Canadian Standards Association, Ontario, Canada.

Della Corte, G., D'Aniello, M., and Landolfo, R., [2013] "Analytical and numerical study of plastic overstrength of shear links," *Journal of Constructional Steel Research*, **82**, 19–32.

Dwairi, H. M. Kowalsky, M. J. and Nau, J. M. [2007] "Equivalent damping in support of direct displacement-based design," *Journal of Earthquake Engineering* **11**(4), 512–530.

EN 1993-1-1:2005. [2005] *Eurocode 3: Design of Steel Structures - Part 1-1: General Rules and Rules for Buildings*. European standard, Comité Européen de Normalisation, Brussels.

EN 1998-1:2004. [2004] *Eurocode 8: Design of Structures for Earthquake Resistance - Part 1: General Rules, Seismic Actions and Rules for Buildings*. European standard, Comité Européen de Normalisation, Brussels.

Engelhardt M. D. and Popov, E. P. [1989] "On design of eccentrically braced frames." *Earthquake Spectra* **5**(3), 495–511. August 1989a. doi: 10.1193/1.1585537.

Engelhardt, M. D. and Popov, E. P. [1989b] "Behavior of long links in eccentrically braced frames." Technical report, Earthquake Engineering Research Center, Berkeley, California.

Faccioli, E., Paolucci, R., and Rey, J. [2004] "Displacement spectra for long periods," *Earthquake Spectra* **20**(2), 347–376.

FEMA P58-1. [2012] *Seismic Performance Assessment of Buildings: Volume 1 - Methodology (P-58-1)*. Technical Report September, Federal Emergency Management Agency, Washington, D.C.

Galvez, P. [2004] Investigation of factors affecting web fractures in shear links. MSc thesis, The University of Texas at Austin.

Goel, S. C. Liao, W. C., Reza Bayat, M., and Chao, S. H. [2009] "Performance-based plastic design (PBPD) method for earthquake-resistant structures: an overview," *The Structural Design of Tall and Special Buildings* **19**(1-2), 115–137.

Grant, D., Blandon, C. A., and Priestley, M. J. N. Modeling inelastic response in direct displacement based design. Technical report, ROSE Report 2005/03, Pavia, Italy, 2005.

Gulkan, P., and Sozen, M. A. [1974] "Inelastic responses of reinforced concrete structures to earthquake motions," *ACI Journal* **71**(12), 604–610.

Hjelmstad, K., and Popov, E. P. [1983] "Seismic behavior of active beam links in eccentrically braced frames," Technical report, Earthquake Engineering Research Center, Berkeley, California.

Jacobsen, L. S. [1930] "Steady forced vibration as influencd by damping," *Transactions of ASME* **52**(15), 169–181.

Kanvinde, A. M. Marshall, K. S., Grilli, D. A., and Bomba, G. [2014] "Forensic analysis of link fractures in eccentrically braced frames during the February 2011 Christchurch earthquake: testing and simulation," *Journal of Structural Engineering* **141**(5), 2014. URL http://ascelibrary.org/doi/10.1061/%328ASCE%29ST.1943-541X.0001043.

Kasai, K. and Popov, E. P. [1986] "A study of seismically resistant eccentrically braced steel frame systems," Technical report, Earthquake Engineering Research Center, Berkeley, California.

Kusyilmaz, A. and Topkaya, C. [2014] "Displacement amplification factors for steel eccentrically braced frames," *Earthquake Engineering and Structural Dynamics*, 2014.

Malakoutian, M., Berman, J. W., and Dusicka, P. [2013] "Seismic response evaluation of the linked column frame system," *Earthquake Engineering & Structural Dynamics* **42**, 795–814.

Maley, T. J., Sullivan, T. J., Lago, A., Roldan, R., and Calvi, G. M. [2013] "Characterising the seismic behavior of steel MRF structures," Technical report, IUSS Press, EUCENTRE Report 2013/02. Pavia, Italy.

Mansour, N. [2010] "Development of the design of eccentrically braced frames with replaceable shear links," PhD. thesis, University of Toronto, 2010.

McKenna, F., Fenves, G., Filippou, F. C., and Mazzoni, S. Open System for Earthquake Engineering Simulation (OpenSees), 2000. URL http://opensees.berkeley.edu/wiki/index.php/Main_Page.

Mohebkhah, A. and Chegeni, B. [2014] "Overstrength and rotation capacity for EBF links made of European IPE sections," *Thin-Walled Structures* **74**, 255–260. January 2014.

Nascimbene, R., Rassati, G. A., and Wijesundara, K.K. [2012] "Numerical simulation of gusset plate connections with rectangular hollow section shape brace under quasi-static cyclic loading," *Journal of Constructional Steel Research* **70**, 177–189.

Nievas, C. I., and Sullivan, T. J. [2015] "Applicability of the Direct Displacement-Based Design Method to Steel Moment Resisting Frames with Setbacks,"*Bulletin of Earthquake Engineering* (June 16). doi:10.1007/s10518-015-9787-1. URL http://link.springer.com/10.1007/s10518-015-9787-1.

NZS 3404. [2007] Steel Structures Standard. New Zealand Standards, Wellington, New Zealand.

Okazaki, T. and Engelhardt, M. D. [2007] "Cyclic loading behavior of EBF links constructed of ASTM A992 steel," *Journal of Constructional Steel Research* **63**(6), 751–765.

Okazaki, T., Engelhardt, M. D., Drolias, A., Schell, E., Hong, J. K., and Uang, C. M. [2009] "Experimental investigation of link-to-column connections in eccentrically braced frames," *Journal of Constructional Steel Research* **65**(7), 1401–1412.

O'Reilly, G. J., and Sullivan, T. J. [2015] "Seismic Design and Assessment of Eccentrically Braced Steel Frame Structures, "Individual Study Thesis, ROSE Programme, UME School, Pavia, Italy.

Pennucci, D., Sullivan, T. J., and Calvi, G. M. [2011] "Displacement reduction factors for the Design of Medium and long period structures," *Journal of Earthquake Engineering* **15**(sup1), 1–29.

Popov, E. P. and Malley, J. O. [1983] "Design of links and beam-to-column connections for eccentrically braced steel frames, Technical report, Earthquake Engineering Research Center, Berkeley, California.

Popov, E. P., Kasai, K., and Engelhardt, M. D. [1987] "Advances in design of eccentrically braced frames," *Earthquake Spectra* **3**(1), 43–55.

Priestley, M. J. N. [1993] "Myths and fallacies in earthquake Engineering—conflicts between design and reality," *Bulletin of the New Zealand Society for Earthquake Engineering* **26**(3), 329–341, 1993.

Priestley, M. J. N., Calvi, G. M., and Kowalsky, M. J. [2007] *Displacement Based Seismic Design of Structures*. IUSS Press, Pavia, Italy.

Roeder, C. W. and Popov, E. P. [1977] "Inelastic behavior of eccentrically braced steel frames under cyclic loadings," Technical report, Earthquake Engineering Research Center, Berkeley, California.

Roldan, R., Welch, D. P., Nievas, C. I., Sullivan, T. J., and Calvi, G. M. [2014] "Guidelines for the performance-based seismic design of steel MRF structures," Technical report, Report EUCENTRE 2014/02, Pavia, Italy.

Ryu, H. C. [2005] "Effects of loading history on the behavior of links in seismic-resistant eccentrically braced frames," MSc thesis, The University of Texas at Austin.

Shibata, A., and Sozen, M. A. [1976] "Substitute-structure method for seismic design in R/C," *Journal of the Structural Division* **102**(1), 1–18.

Sullivan, T. J. [2011] An energy-factor method for the displacement-based seismic design of RC wall structures. *Journal of Earthquake Engineering* **15**(7), 1083–1116.

Sullivan, T. J. [2013a] "Direct displacement-based seismic design of steel eccentrically braced frame structures," *Bulletin of Earthquake Engineering* **11**(6), 2197–2231.

Sullivan, T. J. [2013b] "Highlighting differences between force-based and displacement-based design solutions for RC frame structures," *Structural Engineering International* (2), 112–131.

Sullivan, T. J., Priestley, M. J. N., and Calvi, G. M., Eds. [2012] *A Model Code for the Displacement-Based Seismic Design of Structures - DBD12*. IUSS Press, Pavia, Italy.

Sullivan, T. J., Welch, D. P., and Calvi, G. M. [2014] "Simplified seismic performance assessment and implications for seismic design," *Earthquake Engineering and Engineering Vibration* **13**(Supp1), 95–122.

Tanabashi, R., Kaneta, K., and Ishida, T. [1974] "On the rigidity and ductility of steel bracing assemblages," In *5th World Conference on Earthquake Engineering*, Rome, Italy.

Welch, D. P., Sullivan, T. J., and Calvi, G. M. [2014] "Developing direct displacement-based procedures for simplified loss assessment in performance-based earthquake engineering," *Journal of Earthquake Engineering* **18**(2), 290–322.

Whittaker, A. S., Uang, C. M., and Bertero, V. V. [1987] "Earthquake simulation tests and associated studies of a 0.3 scale model of a six-story eccentrically braced steel structure," Technical report, Earthquake Engineering Research Center, Berkeley, California.